



CERN-EP-2022-072
29 March 2022

ALICE luminosity determination for Pb–Pb collisions at $\sqrt{s_{NN}} = 5.02$ TeV

ALICE Collaboration*

Abstract

Luminosity determination within the ALICE experiment is based on the measurement, in van der Meer scans, of the cross sections for visible processes involving one or more detectors (visible cross sections). In 2015 and 2018, the Large Hadron Collider provided Pb–Pb collisions at a centre-of-mass energy per nucleon pair of $\sqrt{s_{NN}} = 5.02$ TeV. Two visible cross sections, associated with particle detection in the Zero Degree Calorimeter (ZDC) and in the V0 detector, were measured in a van der Meer scan. This article describes the experimental set-up and the analysis procedure, and presents the measurement results. The analysis involves a comprehensive study of beam-related effects and an improved fitting procedure, compared to previous ALICE studies, for the extraction of the visible cross section. The resulting uncertainty of both the ZDC-based and the V0-based luminosity measurement for the full sample is 2.5%. The inelastic cross section for hadronic interactions in Pb–Pb collisions at $\sqrt{s_{NN}} = 5.02$ TeV, obtained by efficiency correction of the V0-based visible cross section, was measured to be 7.67 ± 0.25 b, in agreement with predictions using the Glauber model.

© 2022 CERN for the benefit of the ALICE Collaboration.
Reproduction of this article or parts of it is allowed as specified in the CC-BY-4.0 license.

*See Appendix B for the list of collaboration members

1 Introduction

Cross section measurements at colliders require precise luminosity determination. The rate R of a process can be expressed as

$$R = L\sigma, \quad (1)$$

where L is the luminosity and σ is the process cross section.

In a bunched circular collider, such as the Large Hadron Collider [1] (LHC), the particles circulate in packets (bunches) of finite length, defined by the radio-frequency structure of the accelerator. For two contra-rotating bunches colliding with a null crossing angle, the luminosity can be expressed as

$$L = v_{\text{rev}}N_1N_2 \int f_1(x,y)f_2(x,y)dxdy, \quad (2)$$

where v_{rev} is the accelerator revolution frequency, N_1 and N_2 are the bunch intensities, defined as the number of particles in a bunch, f_1 and f_2 are the probability density distributions of particles in the transverse (x,y) plane for the two bunches (where x is the horizontal direction and y is the vertical direction), assumed to be independent of the longitudinal coordinate z . A detailed discussion of the concept and definition of luminosity can be found in [2].

Assuming factorisation of the density distributions in the two transverse directions, such that

$$f_1(x,y) = f_{1x}(x)f_{1y}(y), \quad f_2(x,y) = f_{2x}(x)f_{2y}(y), \quad (3)$$

one can write

$$L = \frac{v_{\text{rev}}N_1N_2}{h_x h_y}, \quad (4)$$

where

$$h_x = \frac{1}{\int f_{1x}(x)f_{2x}(x)dx} \quad \text{and} \quad h_y = \frac{1}{\int f_{1y}(y)f_{2y}(y)dy} \quad (5)$$

are the effective widths of the beam overlap region.

The van der Meer (vdM) scan [3] is the most common technique employed for luminosity determination at colliders, see, e.g. [4] for a review, and [5–12] for measurements performed at the LHC. In vdM scans, the two beams are moved in the transverse plane, in discrete steps. The rate $R_{\text{vis}}(\Delta x, \Delta y)$ of a reference (visible) process is measured as a function of the transverse beam separations $(\Delta x, \Delta y)$, defined as the distance between the centroids of the beam bunches. The x and y scans are usually performed separately, the beams being head-on (i.e. colliding with zero separation) in the non-scanned direction. In this case, the effective widths h_{x0} and h_{y0} for head-on collisions can be determined as

$$h_{x0} = \frac{\int R_{\text{vis}}(\Delta x, 0)d\Delta x}{R_{\text{vis}}(0, 0)}, \quad h_{y0} = \frac{\int R_{\text{vis}}(0, \Delta y)d\Delta y}{R_{\text{vis}}(0, 0)} \quad (6)$$

(see [3] for a derivation).

When the beams collide with a non-zero crossing angle, Eqs. 2 and 5 need to be modified [2], but it can be shown [13] that the vdM scan technique still allows a precise luminosity determination, and, in particular, that Eqs. 4 and 6 still hold.

The main output of vdM scans is a measurement of the cross section σ_{vis} of the visible process, which can be determined as

$$\sigma_{\text{vis}} = \frac{R_{\text{vis}}(0, 0)h_{x0}h_{y0}}{v_{\text{rev}}N_1N_2} \quad (7)$$

and used for the measurement of luminosity during physics data-taking:

$$L = \frac{R_{\text{vis}}}{\sigma_{\text{vis}}}. \quad (8)$$

The standard vdM scans are typically coupled with a length-scale calibration scan, whose aim is to determine the global conversion factor from the nominal beam displacement to the actual one. In these scans, the two beams are kept at constant separation and moved in consecutive steps in the same direction, and the position of the interaction vertex is measured, using the tracking detectors, as a function of the nominal beam position.

The vdM formalism assumes complete factorisation of the beam profiles in the two transverse directions, such that the beam overlap region is fully described by the product $h_x h_y$. Previous studies performed by ALICE [12, 14–18] and other LHC experiments [6–8, 10, 19] have shown that the actual LHC bunch shapes can violate the factorisation assumption. The size of the effect was found to vary from scan to scan and demanded corrections ranging from the per mil to the percent level. Non-factorisation effects can be studied and quantified by measuring the luminous region parameters, via the distribution of interaction vertices, as a function of the beam separation.

During Run 2, the LHC provided, in 2015 and 2018, lead–lead (Pb–Pb) collisions at a centre-of-mass energy per nucleon pair $\sqrt{s_{\text{NN}}} = 5.02$ TeV. For collisions of lead ions, the visible cross section σ_{vis} seen by a detector (or set of detectors) with a given trigger condition has, in general, two components, one electromagnetic and one hadronic: $\sigma_{\text{vis}} = \epsilon_{\text{EM}} \sigma_{\text{EM}} + \epsilon_{\text{had}} \sigma_{\text{had}}$, where σ_{EM} and σ_{had} are the electromagnetic and hadronic inelastic cross sections and ϵ_{EM} and ϵ_{had} are the fractions of electromagnetic and hadronic inelastic events that satisfy the trigger condition.

The ALICE luminosity determination for the Run 2 Pb–Pb data samples is based on a vdM scan session that took place on November 29, 2018, during the LHC fill ¹ labelled with the number 7483. The visible cross sections for two independent reference processes were measured in this scan session, and used for the indirect luminosity determination of the 2015 and 2018 samples, according to Eq. 8. Note that this procedure does not require a knowledge of ϵ_{had} or ϵ_{EM} .

This document is organised as follows. Section 2 describes the detectors used for the measurement, along with the relevant machine parameters and the procedure adopted for the scan. Section 3 summarises the analysis procedure and presents the results and uncertainties for the visible cross section and luminosity measurement, and for the inelastic hadronic cross section for Pb–Pb collisions at $\sqrt{s_{\text{NN}}} = 5.02$ TeV. The hadronic cross section was determined by combining one of the measured visible cross sections and a data-driven estimate of the corresponding hadronic efficiency ϵ_{had} . Finally, Sec. 4 presents a brief summary of the work.

2 Experimental set-up

In the vdM scan, the cross section was measured for two reference processes, one triggered upon by the Zero Degree Calorimeter (ZDC), the other by the V0 detector. A detailed description of these detectors is given in [20], and their performance is discussed in [21, 22]. The ZDC system features two neutron calorimeters (ZNA, ZNC), located on opposite sides of the ALICE interaction point (IP2), each one at a distance of 112.5 m along the beam axis from IP2, covering the pseudorapidity (η) range $|\eta| > 8.8$. It is completed by two proton calorimeters and two electromagnetic calorimeters, not used for this measurement. The V0 detector consists of two hodoscopes, with 32 scintillator tiles each, located on opposite sides of the interaction region, at distances of 340 cm (V0A) and 90 cm (V0C) along the beam axis from IP2, covering the pseudorapidity ranges $2.8 < \eta < 5.1$ and $-3.7 < \eta < -1.7$, respectively. Note that the LHC beam 1 (2) travels clockwise (anticlockwise) from side A (C) to side C (A).

The ZDC-based visible cross section is defined by a trigger condition, called ZED in the following, which requires a signal in at least one of the two neutron calorimeters, corresponding to an energy

¹A fill is a time interval with continued presence of beam in the accelerator; it starts with the injection and ends with the beam dump.

deposition larger than ~ 1 TeV. Such a threshold is about three standard deviations below the expected signal from a 2.51 TeV neutron. Neutrons are emitted from the fragmentation/evaporation of Pb ions in electromagnetic dissociation events with (single- or double-side) neutron emission, or in hadronic events [23–27]. The trigger condition for the V0-based visible cross section, called VOM in the following, requires the sum of the signal amplitudes from all the V0 scintillators to be above a chosen threshold; during the 2018 Pb–Pb data taking, the threshold was such that the $\sim 50\%$ most central hadronic events were selected, and all electromagnetic events were rejected due to their relatively low particle multiplicity in the V0 acceptance.

The analysis procedure uses, for the length-scale calibration and non-factorisation corrections, the parameters of the luminous region measured via the distribution of interaction vertices, determined with the ALICE Inner Tracking System [28] (ITS).

During the vdM scan session, each Pb beam consisted of 648 bunches, and 619 bunch pairs were colliding at IP2. The minimum spacing between two consecutive bunches in each beam was 100 ns. The β^* value² at IP2 was 0.5 m. The nominal half vertical crossing angle of the two beams at IP2 was about -60 μrad , the minus sign indicating that the two beams exited the crossing region with negative y coordinate with respect to the beam axis³. The current in the ALICE solenoid (dipole) was 30 kA (6 kA), corresponding to a field strength of 0.5 T (0.7 T).

Two pairs of horizontal and vertical scans were performed, to obtain two statistically independent cross section measurements per bunch pair. In each horizontal (vertical) scan, the nominal beam separation Δx (Δy) was varied in 25 equal steps⁴ from -97.3 μm to $+97.3$ μm . A separation of 100 μm corresponds to about six times the root mean square of the transverse beam profile. During each step, the beams were maintained in position for 28 s, and the ZED and VOM trigger counts were integrated in 14 time bins of 2 s each. The counts were measured separately for each colliding bunch pair. In order to provide additional input for non-factorisation studies, two diagonal scans were performed, where the beam separation was varied simultaneously in the two transverse directions. Finally, a set of length-scale calibration scans was performed.

The bunch intensities were of the order of $(7-10)\times 10^7$ Pb ions per bunch. The bunch-intensity measurement was provided by the LHC instrumentation [29]: a direct current transformer (DCCT), measuring the total beam intensity, and a fast beam current transformer (fBCT), measuring the relative bunch intensities. For the relative bunch intensities, data from a second device, the ATLAS beam pick-up system (BPTX [30]) was also used. The accelerator orbit is nominally divided in 3564 slots of 25 ns each. Given the radio-frequency configuration of the LHC, each slot is divided in ten buckets of 2.5 ns each. In nominally filled slots, the so-called main bunch is captured in the central bucket of the slot. Following the convention established in [31], the charge circulating outside of the nominally filled slots is referred to as ghost charge; the charge circulating within a nominally filled slot but not captured in the central bucket is referred to as satellite charge. The ghost and satellite charges do not contribute to the luminosity at the nominal interaction point. Hence, they must be subtracted from the total beam intensity. A measurement of the ghost-charge fraction was provided independently by the LHCb collaboration, via the rate of beam–gas collisions⁵ occurring in nominally empty bunch slots, as described in [10], and by the LHC Longitudinal Density Monitor (LDM), which measures synchrotron radiation photons emitted by the beams [32]. The LDM also provides a measurement of the satellite-charge fraction. For the vdM

²The $\beta(z)$ function describes the single-particle motion and determines the variation of the beam envelope as a function of the coordinate along the beam orbit (z). The transverse size of the beam at a given position along the beam trajectory is proportional to the square root of β . The notation β^* denotes the value of the β function at the interaction point.

³ALICE uses a Cartesian system whose origin is at the LHC Interaction Point 2 (IP2). The z axis is parallel to the mean beam direction at IP2 and points along the LHC Beam 2 (i.e. LHC anticlockwise). The y axis points upwards while the x axis is perpendicular to the y and z axes, forming a right-handed orthogonal system.

⁴See Appendix A for details

⁵A definition of beam–gas collision is provided in Section 3.

scan under analysis, the measured ghost-charge fraction was about 4% (3%) for beam 1 (beam 2) and the bunch-averaged satellite-charge fraction was about 3% for both beams, resulting in a total correction to the bunch intensity product (hence to the cross section) of about 13%. Satellite bunches in a beam may interact with main bunches in the other beam. These events must be identified and subtracted from the measured visible process rates, as will be described in Section 3.

3 Analysis and results

3.1 Visible cross section determination

In previous studies dedicated to the luminosity determination in pp [14–17], p–Pb [12, 18], and Pb–Pb [21] collisions in the ALICE experiment, the trigger rates were measured as a function of the beam separation and corrected for background and pile-up effects. A χ^2 -based fit of the scan curves (separately for the x and y scans) yielded a measurement of $R(0, 0)$, h_{x0} , and h_{y0} , which could be inserted directly into Eq. 7 to determine σ_{vis} . In comparison, e.g. to the studies performed for pp collisions, the present analysis deals with a collision rate per colliding bunch pair lower by about one order of magnitude for ZED and three orders of magnitude for V0M. This demands a different approach, designed to obtain a better treatment of statistical uncertainties at very small numbers of trigger counts. For each colliding bunch pair, the number of triggered events t_i and the number of sampled LHC orbits n_i during time bin i are used as inputs for a binomial likelihood fit:

$$\ln \mathcal{L} = \sum_i [t_i \ln P_i + (n_i - t_i) \ln (1 - P_i)] \quad (9)$$

where P_i is the probability of having a trigger in a bunch crossing, related to the mean number of triggers per bunch crossing μ_i by Poissonian statistics, $P_i = 1 - e^{-\mu_i}$. The quantity μ_i is modelled by the fit function, according to the relations

$$\mu_i = \frac{R_{\text{vis}}(\Delta x_i, \Delta y_i)}{v_{\text{rev}}} + p_{s,i} + \tilde{p}_1 N_{1,i} + \tilde{p}_2 N_{2,i} + p_0 \quad (10)$$

and

$$R_{\text{vis}}(\Delta x_i, \Delta y_i) = v_{\text{rev}} N_{1,i} N_{2,i} \frac{\sigma_{\text{vis}}}{h_{x0} h_{y0}} f(\Delta x_i) g(\Delta y_i), \quad (11)$$

where: $N_{1,i}$ and $N_{2,i}$ are the intensities of the two colliding bunches; Δx_i and Δy_i are the beam separations, corrected for beam–beam deflection [33, 34] and orbit drifts [35, 36], f and g parametrise the luminosity dependence on Δx_i and Δy_i , respectively; h_{x0} and h_{y0} are the integrals of f and g , respectively, divided by their peak values, consistently with Eq. 6; $p_{s,i}$ is the separation-dependent probability that the trigger is fired by a collision between one of the two colliding bunches and a satellite bunch in the other beam, or by the collision of two satellites; \tilde{p}_1 (\tilde{p}_2) is the probability that the trigger is fired by a collision of a bunch of beam 1 (beam 2) with residual gas in the beam pipe (beam–gas collision), normalised by the bunch intensity; p_0 is the probability that the trigger is fired in the absence of beams (detector noise).

The functions $f(\Delta x)$ and $g(\Delta y)$ were chosen to have a Gaussian core with mean value and standard deviation as the only free parameters, the normalisation being constrained by Eq. 7. In order to improve the description of data at large separation, the Gaussian function is modified at absolute separations larger than a certain threshold. For each scan step beyond the threshold, an independent offset is added to Δx_i or Δy_i in the definition of the fitting function, so that there is one additional fit parameter for each of these steps. The threshold is chosen, independently for each colliding bunch pair, as the minimum value allowing one to obtain $\chi^2/ndf \sim 1$; depending on the considered colliding bunch pair and scan, it is located 1.3–2.5 standard deviations away from the peak, and the total number of parameters needed to

describe the tails varies between 7 and 13. The function is constrained to be symmetric around the peak by using the same tail parameter for scan steps at opposite nominal separation. A formal definition of the fitting functions $f(\Delta x)$ and $g(\Delta y)$ is provided in Appendix A.

The parameters p_0 , \tilde{p}_1 and \tilde{p}_2 were estimated by means of an independent fit to the trigger rates in non-colliding and empty bunch slots. Empty bunch slots located immediately after colliding bunch slots were excluded from the fit, because such bunch slots are affected by background from late spurious pulses (after-pulses) and would provide an overestimated measurement of the detector noise. Owing to the minimum spacing of 100 ns between colliding bunches, the contribution from a previous collision to the trigger counts in colliding bunch slots was found to be negligible for both ZED and VOM signals. Because of the large ZDC distance from IP2, the background induced on ZNA (ZNC) by beam–gas collisions of a bunch of beam 1 (2) happening upstream of the calorimeter results in a signal that is 31 bunch slots (~ 750 ns) earlier with respect to nominal beam–beam collisions of that bunch. During the vdM scan, the distribution of Pb-ion bunches along the LHC orbit was such that this background contribution shows up only in nominally empty bunch slots, with no effect on the colliding slots. Therefore, for the ZED analysis, this subset of the empty bunch slots was excluded from the background fit.

The separation-dependent contribution from main–satellite collisions $p_{s,i}$ was evaluated via the signal arrival-time spectra in ZNA and ZNC. The procedure is different for ZED and VOM due to the different selectivity of the two trigger classes. All events triggered by VOM are hadronic and have signals in both ZNA and ZNC. The two-dimensional distribution of arrival times in the two calorimeters for these events is shown in the left panel of Fig. 1. The satellite events are tagged by means of a square cut around the main–main collision peak position, located at (0, 0). Conversely, the ZED trigger has a large contribution from electromagnetic events with single-side neutron emission, so that most of the events have a signal only in one calorimeter. For this sub-sample of ZED-triggered events the estimation of the satellite contamination is based on the one-dimensional arrival time distributions in each of the ZNs, and the fraction of satellite collisions is obtained via a fit of the time distribution to a sum of Gaussian functions, with peak positions fixed to the values expected from the LHC radio-frequency structure (right panel of Fig. 1). The signal from a neutron emitted in a main–satellite collision has the same arrival time as that from a main–main collision if the neutron is emitted by an ion in the main bunch, while it is early or late if the neutron is emitted by an ion in the satellite bunch. Therefore, only half of the neutrons emitted in single-side events from main–satellite collisions are identified as such. Hence, a correction factor of two was applied to the satellite-collision fractions obtained from the single-side neutron event sample.

Due to the dead time of the ZDC detector electronics, the timing information could only be recorded for a fraction of the triggered events. The size of the sample available for the analysis of time spectra does not allow for a statistically significant determination of satellite-collision fractions for each bunch pair and separation step. Therefore, one can only estimate a bunch-averaged satellite contribution. In order to improve the accuracy of the satellite estimation, the fit procedure is therefore extended with a joint likelihood maximisation, based on both timing and trigger data, at each time bin. Let S_i be the number of events identified as main–satellite collisions in T_i recorded events (and t_i the number of trigger counts in n_i sampled orbits, as defined above), the joint binomial likelihood can be written as

$$\ln \mathcal{L}_i = t_i \ln P_i + (n_i - t_i) \ln (1 - P_i) + S_i \ln \left(\frac{P_{s,i}}{P_i} \right) + (T_i - S_i) \ln \left(\frac{P_i - P_{s,i}}{P_i} \right). \quad (12)$$

The maximisation procedure determines the most probable value for $p_{s,i}$ for the measured values of n_i , t_i , T_i and S_i and the current expected P_i . The $p_{s,i}$ value obtained is then fed into the global likelihood according to Eqs. 9 and 10.

In summary, the free parameters of the global likelihood fit for a given colliding bunch pair are the visible cross section, the mean values and standard deviations of the Gaussian cores of the $f(\Delta x)$ and

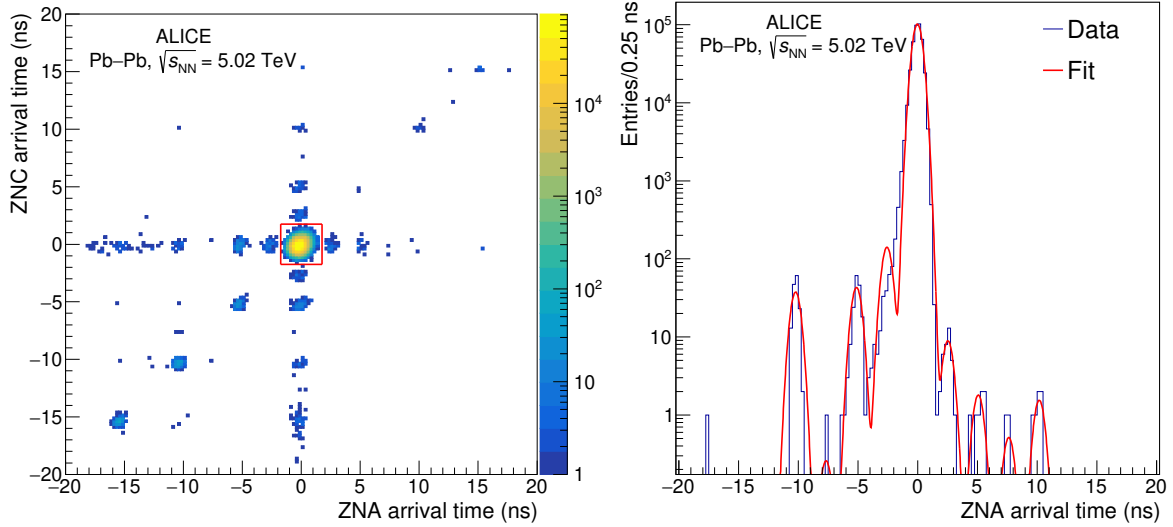


Figure 1: (Colour online) Left: correlation between the arrival times, relative to main–main collisions, of signals in ZNA and ZNC for events triggered by VOM. The square box depicts the satellite–collision rejection cut discussed in the text. Events outside the box are from main–satellite collisions (horizontal and vertical bands) and from satellite–satellite collisions (diagonal band). Right: distribution of the arrival time, relative to main–main collisions, in one of the two neutron calorimeters for ZED-triggered single-side neutron events. The superimposed curve shows a fit with a sum of Gaussian distributions. Both figures are for head-on collisions ($\Delta x = \Delta y = 0$).

$g(\Delta y)$ functions, and 7 to 13 tail parameters for each of the two functions.

As an example, in Fig. 2 the measured trigger probability per bunch crossing as a function of time during the vdM scan is shown for one pair of colliding bunches, together with the expectation from the fit. The values of χ^2/ndf are typically close to unity. As a remark, χ^2/ndf values as large as ~ 2 are obtained if a pure Gaussian function is used, without introducing any tail parameter.

The ZED and VOM analyses provide largely independent estimates of the effective beam widths h_{x0} and h_{y0} , via the fitted parameters of $f(\Delta x)$ and $g(\Delta y)$. The $h_{x0}h_{y0}$ products obtained in the ZED and in the VOM analysis are consistent within 0.13%, which provides an indication that detector-dependent effects such as background and pile-up are under control.

Three length-scale calibration scans were performed for each direction, with different displacement step size, in order to test for a possible dependence on such a parameter. The horizontal (vertical) calibration factor is the slope parameter of a linear fit to the measured horizontal (vertical) vertex displacement versus the nominal one, as illustrated in Fig. 3. The vertex position was determined using tracks reconstructed in the ITS. The resulting (multiplicative) correction factor to the fitted σ_{vis} is the product of the horizontal and vertical calibration factors, and was found to be 0.964 ± 0.010 . The uncertainty has a statistical (0.5%) and a systematic contribution. The latter accounts for deviations from the linear trend in the individual fits (0.3%), for the dependence of the results on the displacement step size (0.4%), and for the dependence of the results on the track and event selection criteria used in the vertex determination procedure (0.7%).

The impact of non-factorisation effects was evaluated by simultaneously fitting the rates and the luminous-region parameters (positions, sizes, transverse tilt) during both the standard and the diagonal scans with a three-dimensional non-factorisable double-Gaussian model [7, 14, 37, 38], and computing the bias on the head-on luminosity with respect to a factorisable model. The resulting (multiplicative) correction factor to the fitted σ_{vis} is 1.011 ± 0.011 , where, conservatively, an uncertainty as large as the correction is

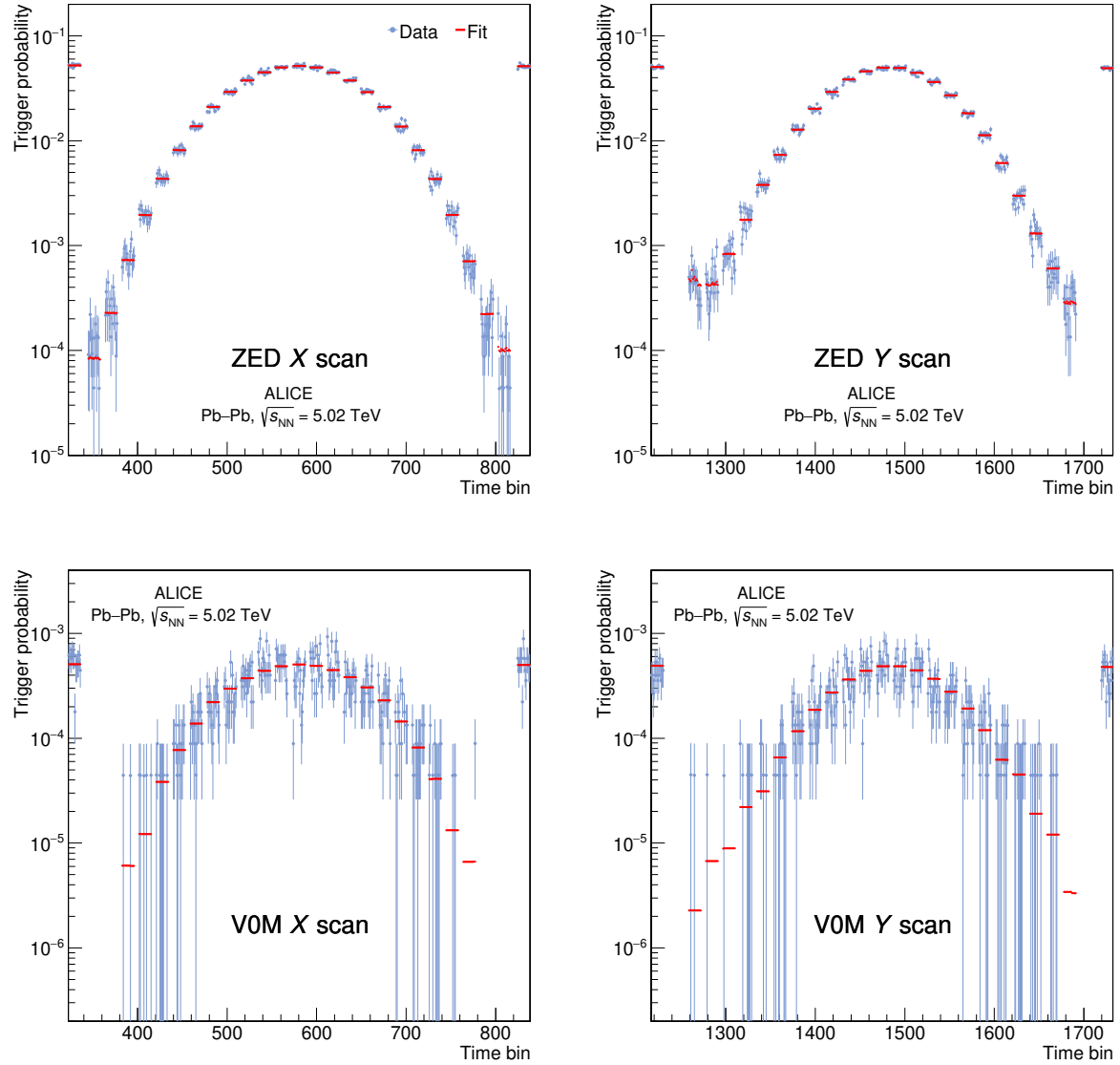


Figure 2: (Colour online) ZED (top) and VOM (bottom) trigger probabilities per bunch crossing for a typical colliding bunch pair, as a function of time, during the first horizontal and vertical vdM scan. Each time bin corresponds to an acquisition window of ~ 2 s. The uncertainties are statistical only. The fit expectation values are also shown, as lines, in each time bin. Time bins during which the beams are being displaced, not considered in the analysis, are not shown.

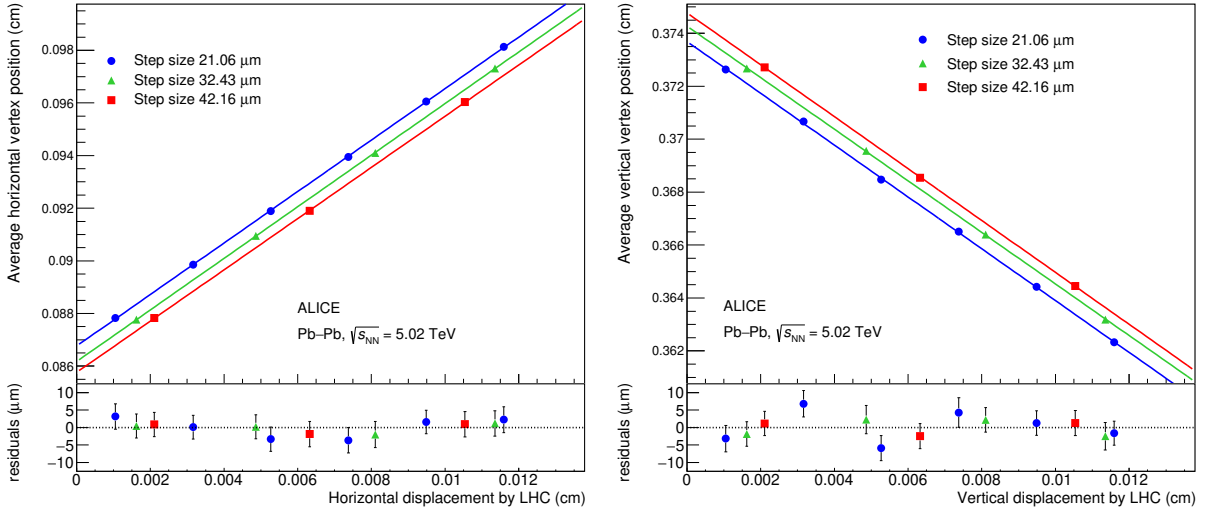


Figure 3: (Colour online) Nominal versus measured displacements in the horizontal (left) and vertical (right) length-scale calibration scans, obtained from events with reconstructed-track multiplicity ranging from 260 to 500. Data are represented by symbols, while a linear fit is represented by the solid lines. The uncertainties are smaller than the symbol sizes. The fit residuals are shown in the lower panel. The blue (green, red) lines and solid circles (triangles, squares) correspond to a nominal displacement step size of 21.06 μm (32.43 μm , 42.16 μm).

assigned, to account for the non-accurate description of some of the luminous-region parameters by the model.

The ZED and VOM cross sections measured for all colliding bunch pairs and scans are shown as a function of the product of bunch intensities $N_1 N_2$ in Fig. 4. For both luminometers and scans, no significant dependence of σ_{vis} on $N_1 N_2$ is observed. However, non-statistical fluctuations of the cross section are present, particularly visible for ZED, which has better statistical precision. In order to take these into account, a systematic uncertainty of 0.1% is assigned, computed as $\sqrt{\chi^2/ndf - 1}$ times the statistical uncertainty of the average cross section [39], where χ^2/ndf is obtained from the constant-value fits to the bunch-by-bunch cross sections shown in Fig. 4. The observed fluctuations are likely related to the significant bunch-by-bunch variation of the satellite-charge fraction (on the order of 50% root mean square, as measured by the LDM). A major contribution to the bunch-by-bunch spread of σ_{vis} was found to originate from pairs with large satellite-charge fraction. A bunch-by-bunch correction for satellite-charge was not performed in this analysis, due to a limited knowledge of the sensitivity of fBCT (or BPTX) to charge in satellite buckets. Instead, the bunch-averaged satellite charge was used as an overall correction to the total beam current measured by DCCT, assuming satellite charge does not contribute to the fBCT signal.

The bunch-averaged cross sections measured in the two scans agree within 1%, which is considered as an additional systematic uncertainty. The measured visible cross sections, obtained by averaging the results from the two scans, are $\sigma_{\text{ZED}} = 420.58 \pm 0.03$ (stat.) b and $\sigma_{\text{VOM}} = 3.933 \pm 0.003$ (stat.) b.

The combined impact of the subtraction of background from beam–gas collisions, electronic noise, and satellite collisions on the final cross section is about 1.5% for ZED and 1% for VOM, largely dominated by satellite collisions. The main source of uncertainty of the satellite-collision background estimation is the usage of bunch-integrated timing data in the evaluation of the satellite collision fractions, with a (potentially limited) sensitivity to bunch-by-bunch variations provided by the joint likelihood minimisation of Eq. 12. An alternative method was tested, where the satellite-collision probability $p_{s,i}$ for a given bunch pair is evaluated as the bunch-integrated satellite-collision fraction S_i/T_i measured with the

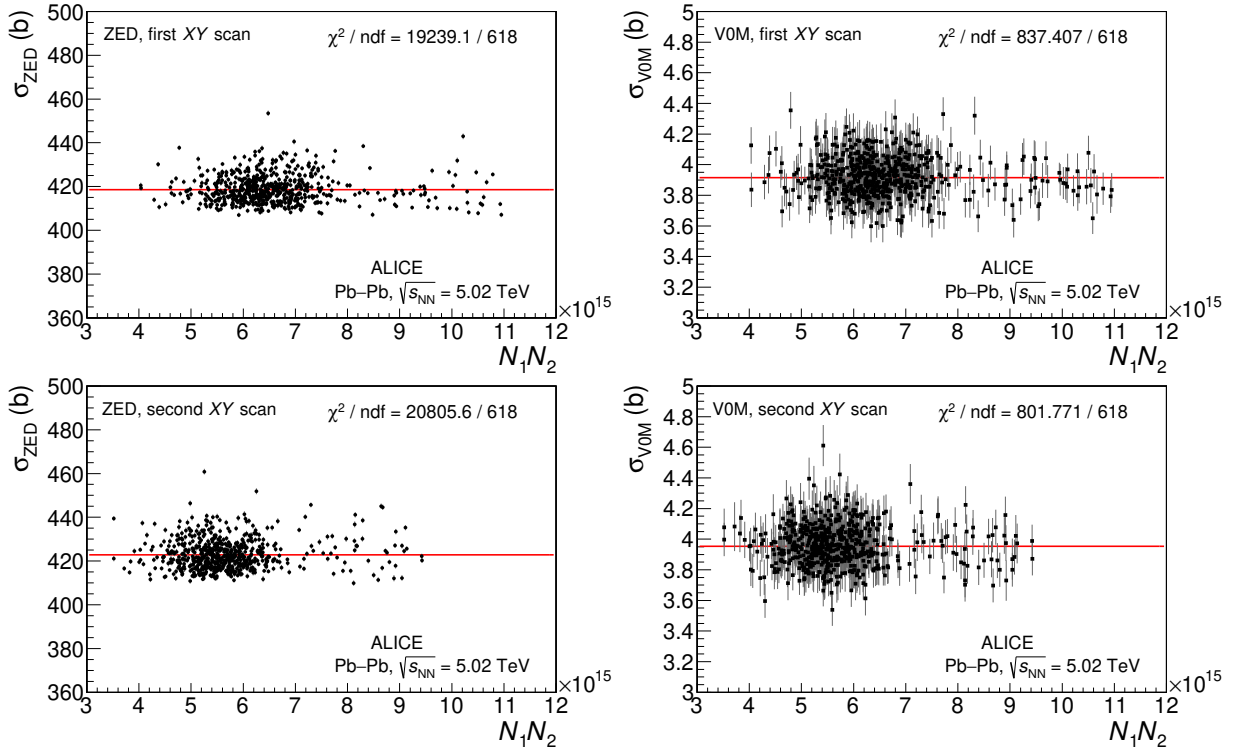


Figure 4: (Colour online) Measured ZED (left) and VOM (right) visible cross sections as a function of the product of the ion bunch intensities, for the first (top) and second vdM scan (bottom). Uncertainties are statistical only. The solid line represents a fit to a constant value.

ZDC timing, scaled by the ratio between the satellite charge fraction for that bunch pair and the bunch-averaged satellite-charge fraction, both measured by the LDM. The systematic uncertainty is estimated as the maximum difference, across scans and luminometers, between the visible cross sections obtained with the standard and alternative method, and amounts to 1.2%. The systematic uncertainty on the subtraction of background from beam–gas and electronic noise is estimated by setting the parameters p_0 , \tilde{p}_1 and \tilde{p}_2 to zero in the likelihood fit (see Eq. 9 and 10). This corresponds to the extreme assumption that all counts in nominally non-colliding bunch slots originate from collisions involving ghost charge. The variation in visible cross section, retained as uncertainty, is 0.3% at most.

The uncertainty of the bunch intensity is 0.8%, from the quadratic sum of three components: 0.5%, from the uncertainty of the total beam current normalisation from the DCCT, evaluated as described in [40]; 0.2%, from the uncertainty of the relative bunch populations, evaluated as the difference between the fBCT- and BPTX-based results; and 0.6%, from the uncertainty of the ghost and satellite charge [10, 32], dominated by the difference between the LHCb and LDM measurements of the ghost-charge fraction. No additional uncertainty is assigned to the bunch-by-bunch spread of satellite charge, because about 95% of the bunches in each beam were colliding in IP2. Under these circumstances, the bunch-pair-averaged visible cross section is essentially driven by the total beam current measurement from DCCT (to which the sum of fBCT signals is normalised), and a non-perfect evaluation of the satellite charge in each bunch slot only leads to a bunch-by-bunch spread of the measured cross sections, with negligible or no bias to the final result, as was verified by making different assumptions for the fBCT sensitivity to satellites.

The measurement of the width of the beam-overlap region in a van der Meer scan can be perturbed by a variation of the bunch emittance during the scan itself. The variation rate of the effective beam widths was estimated with two different methods. The first uses the difference of the measured widths between the first and second scan, the second uses the time evolution of the rate at zero separation, corrected

by the bunch intensity decay. The second method yields larger variation rates (by about 70%) than the first. The potential bias on the measured visible cross sections was estimated in a realistic simulation of the performed scans, assuming an exponential time dependence of the effective beam widths, using the slopes obtained with the second method. The resulting uncertainty is 0.5%.

Possible non-linearities in the steering magnet behaviour during the scan, e.g. due to hysteresis, were considered as a source of systematic uncertainty. A preliminary hysteresis model [41] developed for the LHC was used. The model provides, for each scan step and for both beams, an upper limit to the hysteresis-induced shift of the beam position with respect to its nominal value. For this fill, the maximum shift is about $0.5 \mu\text{m}$. In order to estimate a possible bias on the cross section, the fit of Eq. 9 was performed with the separation at each step modified according to the predicted position shift of both beams. The change in average visible cross section is 0.2% for both luminometers and is retained as a systematic uncertainty.

The uncertainty of the orbit-drift correction was conservatively taken to be as large as the effect of the correction (0.15%). The uncertainty of the beam–beam deflection correction was evaluated by varying the input parameters to the deflection calculation within a reasonable range, as described in [14], and found to be less than 0.1%. The effect of distortions of the bunch shapes due to the mutual interaction between the two beams was also evaluated, within the framework outlined in [34], and found to be less than 0.1%.

The systematic uncertainty associated with the choice of the fitting strategy was evaluated: by varying the range of beam separations described by the Gaussian core (varying thereby the number of fit parameters used to describe the tails); by discarding the last scan step, where the satellite contribution is dominant; and by extracting the visible cross section from a simultaneous fit to all colliding bunch pairs, with common shape parameters, instead of averaging the results from individual fits. The resulting uncertainty is 0.4%.

The total systematic uncertainty of the visible cross section measurement, obtained as the quadratic sum of the contributions listed above, amounts to 2.4% for both ZED and VOM.

3.2 Hadronic inelastic cross section determination

As an additional output of the vdM scan analysis, the inelastic hadronic cross section σ_{had} was determined by correcting the visible cross section σ_{VOM} for the VOM trigger efficiency. The ALICE centrality determination framework [42, 43] assigns to each event a centrality value, based on the total signal amplitude in the V0 detector. The centrality is defined as the probability that a hadronic Pb–Pb collision results in an amplitude larger than the measured value. The centrality calibration for the 2018 sample was performed using a minimum-bias trigger requiring a signal in each of V0A, V0C, ZNA and ZNC. Such a trigger is fully efficient for hadronic events and free from electromagnetic contamination for the $\sim 90\%$ most central events [44, 45]. In order to obtain the shape of the amplitude spectrum in the most peripheral events, the minimum-bias-triggered spectrum is fitted with a Monte Carlo implementation of the Glauber model [46], coupled with a two-component ancestor model for particle production; the fit is performed above a chosen amplitude threshold (anchor point, corresponding to a centrality of 90%), where no trigger bias is expected. The centrality distribution of VOM-triggered events, determined using the framework described above, is shown in Fig. 5. The distribution is uniform in the 0–50% centrality range, where the VOM trigger is fully efficient, then drops rapidly to zero in the range 50–52%. When the distribution is normalised such that its integral in 0–50% is 0.5, its total integral provides the VOM efficiency for hadronic interactions, ϵ_{had} . For the fill in which the vdM scan was performed, this procedure results in $\epsilon_{\text{had}} = 0.513 \pm 0.012$. The quoted uncertainty is systematic and is obtained as the quadratic sum of two components. The first one, of 1.4%, was determined, similar to what was done in Ref. [44], by varying the centrality at the anchor point within $\pm 1\%$ (referring here to an absolute variation, i.e., from 89% to 91%). The second one, of 1.8%, was determined as the difference between the default efficiency

value and the one obtained by fitting the V0 amplitude spectrum with a different template, based on the T_RENTo model [47]. Finally, one has

$$\sigma_{\text{had}} = \frac{\sigma_{\text{V0M}}}{\epsilon_{\text{had}}} = 7.67 \pm 0.25 \text{ b},$$

where the quoted uncertainty is the combination of the statistical and systematic uncertainties of the visible cross section, of 2.4%, and of the trigger efficiency, of 2.3%. The measured cross section is in agreement with the prediction of (7.62 ± 0.15) b from Ref. [48], based on a Monte Carlo implementation of the Glauber model with a nuclear radius of ~ 6.7 fm, a nuclear skin depth for protons (neutrons) of ~ 0.45 fm (~ 0.56 fm), and an inelastic nucleon–nucleon cross section of ~ 67 mb.

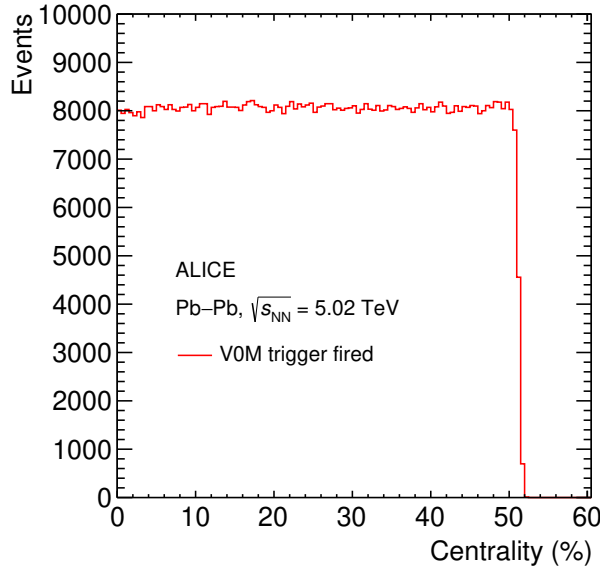


Figure 5: Centrality distribution of events satisfying the V0M trigger condition, for the LHC fill during which the vdM scan was performed.

3.3 Consistency and stability of the luminosity calibration

In order to test the stability and mutual consistency of the ZED and V0M calibrations, the luminosities measured with the two reference signals throughout the whole 2015 and 2018 data-taking periods were compared on a run-by-run basis. In the ALICE nomenclature, a run is a set of data collected within a start and a stop of the data acquisition, under stable detector and trigger configurations⁶. For each run, the trigger counts, integrated over colliding bunch slots, were corrected by subtracting the estimated beam–gas background, detector noise, and background from main–satellite collisions. As explained earlier, the beam–gas background was estimated by means of the counts in non-colliding bunch slots, rescaled by the relative fractions of beam intensities; the contribution from detector noise was estimated via the counts in empty slots; the background from main–satellite collisions was estimated using the ZDC timing data. For each run, the pile-up corrected ratio between the V0M- and ZED-based luminosities was computed from the corrected number of trigger counts N_{V0M} and N_{ZED} and from the total number of bunch crossings in the run N_{BC} as

$$\frac{L_{\text{V0M}}}{L_{\text{ZED}}} = \frac{\ln(1 - N_{\text{V0M}}/N_{\text{BC}})\sigma_{\text{ZED}}}{\ln(1 - N_{\text{ZED}}/N_{\text{BC}})\sigma_{\text{V0M}}}. \quad (13)$$

While the ZED trigger settings remained unchanged throughout the 2015 and 2018 data-taking periods, the threshold for the V0M trigger was different in 2015 and 2018. Furthermore, in 2018, the threshold

⁶For the data-taking period under consideration, the duration of a run ranges from ~ 5 minutes to ~ 7 hours.

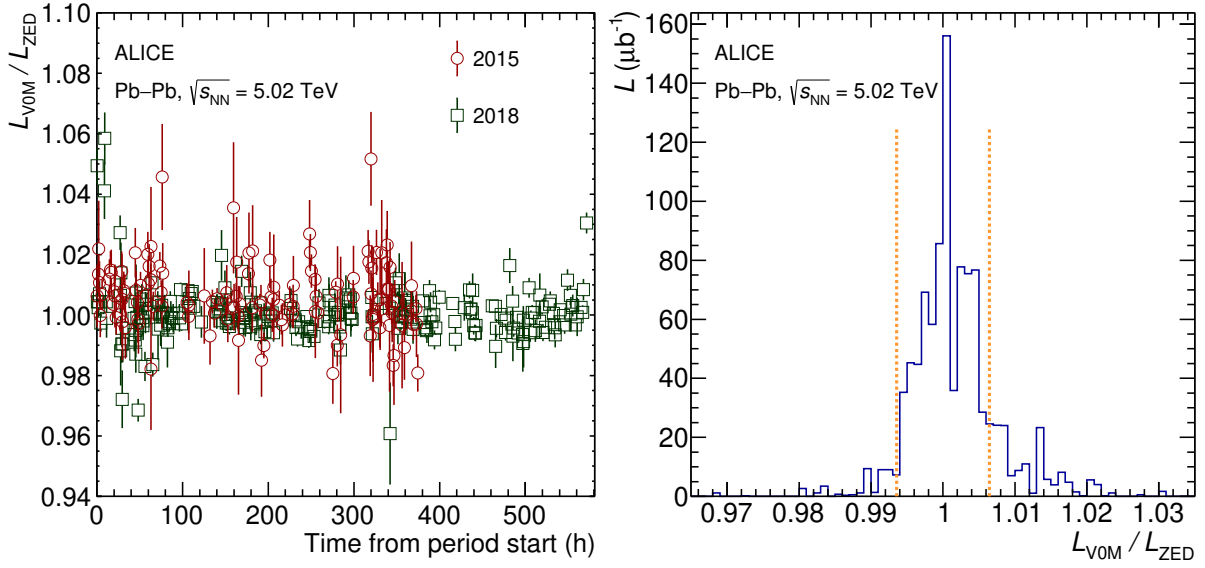


Figure 6: (Colour online) Left: ratio of VOM and ZED luminosities calculated according to Eq. 13 as a function of time with respect to the beginning of the data-taking periods for 2015 (circles) and 2018 (squares). The uncertainties are statistical. Right: distribution of the ratios for all runs (2015 and 2018), weighted with the run luminosity. The dashed vertical lines are located at $L_{\text{VOM}}/L_{\text{ZED}} = 1 \pm \alpha$, where $\alpha \sim 0.007$ is the mean quadratic difference from unity.

was slightly adjusted a few times during data-taking as the VOM-based centrality trigger was being tuned. For the data-taking periods with different threshold settings with respect to the vdM scan, the VOM trigger efficiency was re-determined with the procedure described earlier, and the VOM cross section re-scaled by the ratio of the measured efficiency to that measured in the fill containing the van der Meer scans.

The luminosity ratio as a function of time and the distribution of the ratio values over all runs, weighted with the run luminosity, are shown in Fig. 6. The mean quadratic difference of the ratio from unity is about 0.7% and is retained as a systematic uncertainty of the stability and mutual consistency of the luminosity calibration. When the analysis is restricted to the 2015 or 2018 sample, the mean quadratic difference from unity amounts to 1% or 0.5%, respectively.

3.4 Luminosity uncertainty

In Table 1 a summary of the different contributions to the uncertainty of the visible cross section and the luminosity measurement is presented. The luminosity uncertainty, obtained as the quadratic sum of the visible cross section uncertainty and of the stability and consistency uncertainty, amounts to 2.5% for both ZED and VOM. For the sake of comparison, the luminosity uncertainty obtained by ALICE for Pb–Pb collisions at $\sqrt{s_{\text{NN}}} = 2.76$ TeV (LHC Run 1) was of 5–6% [21].

4 Conclusions

In 2015 and 2018, the ALICE Collaboration took data with Pb–Pb collisions at a centre-of-mass energy $\sqrt{s_{\text{NN}}} = 5.02$ TeV. In order to provide a reference for the luminosity determination, vdM scans were performed and visible cross sections were measured for two processes, ZED (neutron emission in the acceptance of the neutron Zero Degree Calorimeters) and VOM (energy deposition in the V0 detector by events up to $\sim 50\%$ centrality). Each of the two detectors provides a measurement of the luminosity with a total uncertainty, for the full sample (2015 and 2018), of 2.5%. These uncertainties improve by about a factor of two with respect to those obtained by ALICE in previous studies dedicated to Pb–Pb

Table 1: Relative uncertainties of the measurement of visible cross sections and luminosity in Pb–Pb collisions at $\sqrt{s_{NN}} = 5.02$ TeV. The stability and consistency and the total luminosity uncertainties refer to the full Run 2 sample (2015 and 2018); uncertainties for the single periods are given in the text.

Source	Uncertainty (%)	
	ZED	VOM
Statistical	0.008	0.08
$h_{x0}h_{y0}$ consistency (VOM vs ZED)	0.13	
Length-scale calibration	1	
Non-factorisation	1.1	
Bunch-to-bunch consistency	0.1	
Scan-to-scan consistency	1	
Satellite collisions	1.2	
Beam–gas and noise	0.3	
Bunch intensity	0.8	
Emittance variation	0.5	
Magnetic non-linearities	0.2	
Orbit drift	0.15	
Beam–beam deflection and distortion	0.1	
Fitting scheme	0.4	
Total of visible cross section	2.4	
Stability and consistency	0.7	
Total of luminosity	2.5	2.5

collisions at $\sqrt{s_{NN}} = 2.76$ TeV. The inelastic cross section for hadronic interactions in Pb–Pb collisions at $\sqrt{s_{NN}} = 5.02$ TeV, obtained by trigger-efficiency correction of the VOM cross section, was measured to be 7.67 ± 0.25 b, in agreement with predictions from the Glauber model.

Acknowledgements

The ALICE Collaboration would like to thank all its engineers and technicians for their invaluable contributions to the construction of the experiment and the CERN accelerator teams for the outstanding performance of the LHC complex. The ALICE Collaboration gratefully acknowledges the resources and support provided by all Grid centres and the Worldwide LHC Computing Grid (WLCG) collaboration. The ALICE Collaboration acknowledges the following funding agencies for their support in building and running the ALICE detector: A. I. Alikhanyan National Science Laboratory (Yerevan Physics Institute) Foundation (ANSL), State Committee of Science and World Federation of Scientists (WFS), Armenia; Austrian Academy of Sciences, Austrian Science Fund (FWF): [M 2467-N36] and Nationalstiftung für Forschung, Technologie und Entwicklung, Austria; Ministry of Communications and High Technologies, National Nuclear Research Center, Azerbaijan; Conselho Nacional de Desenvolvimento Científico e Tecnológico (CNPq), Financiadora de Estudos e Projetos (Finep), Fundação de Amparo à Pesquisa do Estado de São Paulo (FAPESP) and Universidade Federal do Rio Grande do Sul (UFRGS), Brazil; Bulgarian Ministry of Education and Science, within the National Roadmap for Research Infrastructures 2020-2027 (object CERN), Bulgaria; Ministry of Education of China (MOEC), Ministry of Science & Technology of China (MSTC) and National Natural Science Foundation of China (NSFC), China; Ministry of Science and Education and Croatian Science Foundation, Croatia; Centro de Aplicaciones Tecnológicas y Desarrollo Nuclear (CEADEN), Cubaenergía, Cuba; Ministry of Education, Youth and Sports of the Czech Republic, Czech Republic; The Danish Council for Independent Research | Natural Sciences, the VILLUM FONDEN and Danish National Research Foundation (DNRF),

Denmark; Helsinki Institute of Physics (HIP), Finland; Commissariat à l’Energie Atomique (CEA) and Institut National de Physique Nucléaire et de Physique des Particules (IN2P3) and Centre National de la Recherche Scientifique (CNRS), France; Bundesministerium für Bildung und Forschung (BMBF) and GSI Helmholtzzentrum für Schwerionenforschung GmbH, Germany; General Secretariat for Research and Technology, Ministry of Education, Research and Religions, Greece; National Research, Development and Innovation Office, Hungary; Department of Atomic Energy Government of India (DAE), Department of Science and Technology, Government of India (DST), University Grants Commission, Government of India (UGC) and Council of Scientific and Industrial Research (CSIR), India; National Research and Innovation Agency - BRIN, Indonesia; Istituto Nazionale di Fisica Nucleare (INFN), Italy; Japanese Ministry of Education, Culture, Sports, Science and Technology (MEXT) and Japan Society for the Promotion of Science (JSPS) KAKENHI, Japan; Consejo Nacional de Ciencia (CONACYT) y Tecnología, through Fondo de Cooperación Internacional en Ciencia y Tecnología (FONCICYT) and Dirección General de Asuntos del Personal Académico (DGAPA), Mexico; Nederlandse Organisatie voor Wetenschappelijk Onderzoek (NWO), Netherlands; The Research Council of Norway, Norway; Commission on Science and Technology for Sustainable Development in the South (COMSATS), Pakistan; Pontificia Universidad Católica del Perú, Peru; Ministry of Education and Science, National Science Centre and WUT ID-UB, Poland; Korea Institute of Science and Technology Information and National Research Foundation of Korea (NRF), Republic of Korea; Ministry of Education and Scientific Research, Institute of Atomic Physics, Ministry of Research and Innovation and Institute of Atomic Physics and University Politehnica of Bucharest, Romania; Ministry of Education, Science, Research and Sport of the Slovak Republic, Slovakia; National Research Foundation of South Africa, South Africa; Swedish Research Council (VR) and Knut & Alice Wallenberg Foundation (KAW), Sweden; European Organization for Nuclear Research, Switzerland; Suranaree University of Technology (SUT), National Science and Technology Development Agency (NSTDA), Thailand Science Research and Innovation (TSRI) and National Science, Research and Innovation Fund (NSRF), Thailand; Turkish Energy, Nuclear and Mineral Research Agency (TENMAK), Turkey; National Academy of Sciences of Ukraine, Ukraine; Science and Technology Facilities Council (STFC), United Kingdom; National Science Foundation of the United States of America (NSF) and United States Department of Energy, Office of Nuclear Physics (DOE NP), United States of America. In addition, individual groups or members have received support from: Marie Skłodowska Curie, Strong 2020 - Horizon 2020, European Research Council (grant nos. 824093, 896850, 950692), European Union; Academy of Finland (Center of Excellence in Quark Matter) (grant nos. 346327, 346328), Finland; Programa de Apoyos para la Superación del Personal Académico, UNAM, Mexico.

References

- [1] L. Evans and P. Bryant, “LHC Machine”, *JINST* **3** (2008) S08001.
- [2] W. Herr and B. Muratori, “Concept of luminosity”, in *CERN Accelerator School and DESY Zeuthen: Accelerator Physics*, pp. 361–367. September, 2003.
<https://cds.cern.ch/record/941318>.
- [3] S. van der Meer, “Calibration of the effective beam height in the ISR”, Tech. Rep. CERN-ISR-PO-68-31, CERN, 1968. <http://cds.cern.ch/record/296752>.
- [4] P. Grafström and W. Kozanecki, “Luminosity determination at proton colliders”, *Prog. Part. Nucl. Phys.* **81** (2015) 97–148.
- [5] ATLAS Collaboration, G. Aad *et al.*, “Luminosity determination in pp collisions at $\sqrt{s} = 7$ TeV using the ATLAS detector at the LHC”, *Eur. Phys. J. C* **71** (2011) 1630, [arXiv:1101.2185](https://arxiv.org/abs/1101.2185) [hep-ex].

- [6] **ATLAS** Collaboration, G. Aad *et al.*, “Improved luminosity determination in pp collisions at $\sqrt{s} = 7$ TeV using the ATLAS detector at the LHC”, *Eur. Phys. J. C* **73** (2013) 2518, arXiv:1302.4393 [hep-ex].
- [7] **ATLAS** Collaboration, M. Aaboud *et al.*, “Luminosity determination in pp collisions at $\sqrt{s} = 8$ TeV using the ATLAS detector at the LHC”, *Eur. Phys. J. C* **76** (2016) 653, arXiv:1608.03953 [hep-ex].
- [8] **CMS** Collaboration, A. M. Sirunyan *et al.*, “Precision luminosity measurement in proton-proton collisions at $\sqrt{s} = 13$ TeV in 2015 and 2016 at CMS”, *Eur. Phys. J. C* **81** (2021) 800, arXiv:2104.01927 [hep-ex].
- [9] **LHCb** Collaboration, R. Aaij *et al.*, “Absolute luminosity measurements with the LHCb detector at the LHC”, *JINST* **7** (2012) P01010, arXiv:1110.2866 [hep-ex].
- [10] **LHCb** Collaboration, R. Aaij *et al.*, “Precision luminosity measurements at LHCb”, *JINST* **9** (2014) P12005, arXiv:1410.0149 [hep-ex].
- [11] **ALICE** Collaboration, B. Abelev *et al.*, “Measurement of inelastic, single- and double-diffraction cross sections in proton–proton collisions at the LHC with ALICE”, *Eur. Phys. J. C* **73** (2013) 2456, arXiv:1208.4968 [hep-ex].
- [12] **ALICE** Collaboration, B. Abelev *et al.*, “Measurement of visible cross sections in proton-lead collisions at $\sqrt{s_{NN}} = 5.02$ TeV in van der Meer scans with the ALICE detector”, *JINST* **9** (2014) P11003, arXiv:1405.1849 [nucl-ex].
- [13] V. Balagura, “Notes on van der Meer Scan for Absolute Luminosity Measurement”, *Nucl. Instrum. Meth. A* **654** (2011) 634–638, arXiv:1103.1129 [physics.ins-det].
- [14] **ALICE** Collaboration, J. Adam *et al.*, “ALICE luminosity determination for pp collisions at $\sqrt{s} = 13$ TeV”, Tech. Rep. ALICE-PUBLIC-2016-002, CERN, 2016. <https://cds.cern.ch/record/2160174/>.
- [15] **ALICE** Collaboration, S. Acharya *et al.*, “ALICE luminosity determination for pp collisions at $\sqrt{s} = 8$ TeV”, Tech. Rep. ALICE-PUBLIC-2017-002, CERN, 2017. <https://cds.cern.ch/record/2255216/>.
- [16] **ALICE** Collaboration, J. Adam *et al.*, “ALICE luminosity determination for pp collisions at $\sqrt{s} = 5$ TeV”, Tech. Rep. ALICE-PUBLIC-2016-005, CERN, 2016. <https://cds.cern.ch/record/2202638/>.
- [17] **ALICE** Collaboration, S. Acharya *et al.*, “ALICE 2017 luminosity determination for pp collisions at $\sqrt{s} = 5$ TeV”, Tech. Rep. ALICE-PUBLIC-2018-014, CERN, 2018. <https://cds.cern.ch/record/2648933/>.
- [18] **ALICE** Collaboration, S. Acharya *et al.*, “ALICE luminosity determination for p-Pb collisions at $\sqrt{s_{NN}} = 8.16$ TeV”, Tech. Rep. ALICE-PUBLIC-2018-002, CERN, 2018. <https://cds.cern.ch/record/2314660/>.
- [19] **CMS** Collaboration, “CMS Luminosity Based on Pixel Cluster Counting - Summer 2013 Update”, Tech. Rep. CMS-PAS-LUM-13-001, CERN, 2013. <https://cds.cern.ch/record/1598864/>.
- [20] **ALICE** Collaboration, K. Aamodt *et al.*, “The ALICE experiment at the CERN LHC”, *JINST* **3** (2008) S08002.

- [21] ALICE Collaboration, B. Abelev *et al.*, “Performance of the ALICE Experiment at the CERN LHC”, *Int. J. Mod. Phys. A* **29** (2014) 1430044, arXiv:1402.4476 [nucl-ex].
- [22] ALICE Collaboration, E. Abbas *et al.*, “Performance of the ALICE VZERO system”, *JINST* **8** (2013) P10016, arXiv:1306.3130 [nucl-ex].
- [23] A. J. Baltz, M. J. Rhoades-Brown, and J. Weneser, “Heavy-ion partial beam lifetimes due to Coulomb induced processes”, *Physical Review E* **54** (1996) 4233.
- [24] ALICE Collaboration, B. Abelev *et al.*, “Measurement of the Cross Section for Electromagnetic Dissociation with Neutron Emission in Pb–Pb Collisions at $\sqrt{s_{NN}} = 2.76$ TeV”, *Phys. Rev. Lett.* **109** (2012) 252302, arXiv:1203.2436 [nucl-ex].
- [25] I. A. Pshenichnov, J. P. Bondorf, I. N. Mishustin, A. Ventura, and S. Masetti, “Mutual heavy ion dissociation in peripheral collisions at ultrarelativistic energies”, *Phys. Rev. C* **64** (2001) 024903, arXiv:nucl-th/0101035.
- [26] I. A. Pshenichnov, “Electromagnetic excitation and fragmentation of ultrarelativistic nuclei”, *Phys. Part. Nucl.* **42** (2011) 215–250.
- [27] M. Broz, J. G. Contreras, and J. D. Tapia Takaki, “A generator of forward neutrons for ultra-peripheral collisions: n_0^n ”, *Comput. Phys. Commun.* **253** (2020) 107181, arXiv:1908.08263 [nucl-th].
- [28] ALICE Collaboration, K. Aamodt *et al.*, “Alignment of the ALICE Inner Tracking System with cosmic-ray tracks”, *JINST* **5** (2010) P03003, arXiv:1001.0502 [physics.ins-det].
- [29] J. J. Gras, D. Belohrad, M. Ludwig, P. Odier, and C. Barschel, “Optimization of the LHC beam current transformers for accurate luminosity determination”, Tech. Rep. CERN-ATS-2011-063, CERN, 2011. <http://cds.cern.ch/record/1379466>.
- [30] C. Ohm and T. Pauly, “The ATLAS beam pick-up based timing system”, *Nucl. Instrum. Meth. A* **623** (2010) 558–560, arXiv:0905.3648 [physics.ins-det].
- [31] A. Alici *et al.*, “Study of the LHC ghost charge and satellite bunches for luminosity calibration”, Tech. Rep. CERN-ATS-Note-2012-029 PERF, CERN, 2012. <https://cds.cern.ch/record/1427728>.
- [32] A. Boccardi, E. Bravin, M. Ferro-Luzzi, S. Mazzoni, and M. Palm, “LHC Luminosity calibration using the Longitudinal Density Monitor”, Tech. Rep. CERN-ATS-Note-2013-034 TECH, CERN, 2013. <https://cds.cern.ch/record/1556087>.
- [33] W. Kozanecki, T. Pieloni, and J. Wenninger, “Observation of Beam-beam Deflections with LHC Orbit Data”, Tech. Rep. CERN-ACC-NOTE-2013-0006, CERN, 2013. <https://cds.cern.ch/record/1581723>.
- [34] V. Balagura, “Van der Meer scan luminosity measurement and beam–beam correction”, *Eur. Phys. J. C* **81** (2021) 26, arXiv:2012.07752 [hep-ex].
- [35] D. Bishop, C. Boccard, E. Calvo-Giraldo, D. Cocq, L. Jensen, R. Jones, J. J. Savioz, and G. Waters, “The LHC Orbit and Trajectory System”, Tech. Rep. CERN-AB-2003-057-BDI, 2003. <https://cds.cern.ch/record/624190>.
- [36] J. Wenninger, “Dispersion Free Steering for YASP and dispersion correction for TI8”, Tech. Rep. LHC-Performance-Note-005, CERN, 2009. <http://cds.cern.ch/record/1156142>.

- [37] S. N. Webb, *Factorisation of beams in van der Meer scans and measurements of the ϕ_{η}^* distribution of $Z \rightarrow e^+e^-$ events in pp collisions at $\sqrt{s} = 8$ TeV with the ATLAS detector*. PhD thesis, Manchester U., 2015-06-01.
<https://inspirehep.net/record/1381312/files/CERN-THESIS-2015-054.pdf>.
- [38] ATLAS Collaboration, “Luminosity determination in pp collisions at $\sqrt{s} = 13$ TeV using the ATLAS detector at the LHC”, Tech. Rep. ATLAS-CONF-2019-021, CERN, 2019.
<https://cdsweb.cern.ch/record/2677054/>.
- [39] Particle Data Group Collaboration, P. A. Zyla *et al.*, “Review of Particle Physics”, *PTEP* **2020** (2020) 083C01.
- [40] C. Barschel, M. Ferro-Luzzi, J.-J. Gras, M. Ludwig, P. Odier, and S. Thoulet, “Results of the LHC DCCT Calibration Studies”, Tech. Rep. CERN-ATS-Note-2012-026 PERF, CERN, 2012.
<https://cds.cern.ch/record/1425904>.
- [41] M. Hostettler and E. Todesco. presentations to the LHC Luminosity Calibration and Measurement Working group (16 November 2020) <https://indico.cern.ch/event/975528/>, and private communication (9 December 2020).
- [42] ALICE Collaboration, B. Abelev *et al.*, “Centrality determination of Pb-Pb collisions at $\sqrt{s_{\text{NN}}} = 2.76$ TeV”, *Phys. Rev. C* **88** (2013) 044909, arXiv:1301.4361 [nucl-ex].
- [43] ALICE Collaboration, S. Acharya *et al.*, “Centrality determination in heavy ion collisions”, Tech. Rep. ALICE-PUBLIC-2018-011, CERN, 2018. <https://cds.cern.ch/record/2636623/>.
- [44] ALICE Collaboration, J. Adam *et al.*, “Centrality Dependence of the Charged-Particle Multiplicity Density at Midrapidity in Pb-Pb Collisions at $\sqrt{s_{\text{NN}}} = 5.02$ TeV”, *Phys. Rev. Lett.* **116** (2016) 222302, arXiv:1512.06104 [nucl-ex].
- [45] ALICE Collaboration, J. Adam *et al.*, “Centrality dependence of the charged-particle multiplicity density at midrapidity in Pb-Pb collisions at $\sqrt{s_{\text{NN}}} = 5.02$ TeV”, Tech. Rep. ALICE-PUBLIC-2015-008, CERN, 2015. <https://cds.cern.ch/record/2118084/>.
- [46] M. L. Miller, K. Reygers, S. J. Sanders, and P. Steinberg, “Glauber modeling in high energy nuclear collisions”, *Ann. Rev. Nucl. Part. Sci.* **57** (2007) 205–243, arXiv:nucl-ex/0701025.
- [47] J. S. Moreland, J. E. Bernhard, and S. A. Bass, “Alternative ansatz to wounded nucleon and binary collision scaling in high-energy nuclear collisions”, *Phys. Rev. C* **92** (2015) 011901, arXiv:1412.4708 [nucl-th].
- [48] D. d’Enterria and C. Loizides, “Progress in the Glauber model at collider energies”, *Ann. Rev. Nucl. Part. Sci.* **71** (2021) 315–44, arXiv:2011.14909 [hep-ph].

A Fitting function definition

The luminosity dependence on the horizontal separation is parametrised (see Eq. 11) with the fitting function $f(\Delta x)$.

With 25 scan steps, one can choose $-12 \leq j \leq +12$, so that the nominal separation at step j is given by

$$\Delta x_{\text{nom},j} = \frac{j}{24}(\Delta x_{\text{nom},\text{max}} - \Delta x_{\text{nom},\text{min}}), \quad (\text{A.1})$$

where $\Delta x_{\text{nom},\text{max}} = -\Delta x_{\text{nom},\text{min}} = 97.3 \mu\text{m}$, and $j = 0$ denotes the (nominal) zero separation. As discussed in Section 3, the actual separation Δx_j is obtained by correcting the nominal separation $\Delta x_{\text{nom},j}$ for the orbit drift and beam–beam deflection effects.

With the above convention, the fitting function is defined as

$$f(\Delta x_j) = e^{-\frac{(\Delta x_j - \mu + \delta_j)^2}{2\sigma^2}}, \quad (\text{A.2})$$

with

$$\delta_j = \delta_{-j} \quad (\text{A.3})$$

and

$$\delta_j = 0 \text{ for } |j| < j_0, \quad (\text{A.4})$$





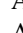





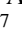

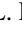





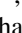
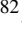

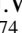
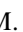


where $j_0 > 0$ is the threshold chosen for the transition between the Gaussian core and the tail (see Section 3 for details). The fit parameters in the function are the mean value μ , the standard deviation σ and the offsets δ_j (with $j_0 < j \leq 12$).

The definition of the function $g(\Delta y)$ used to parametrise the luminosity dependence on the vertical separation is identical, with independent offset parameters.





Depending on the considered colliding bunch pair, the fitting functions use $6 \leq j_0 \leq 9$.

B The ALICE Collaboration

S. Acharya ^{123,131}, D. Adamová ⁸⁵, A. Adler⁶⁹, G. Aglieri Rinella ³², M. Agnello ²⁹, N. Agrawal ⁵⁰, Z. Ahammed ¹³¹, S. Ahmad ¹⁵, S.U. Ahn ⁷⁰, I. Ahuja ³⁷, A. Akindinov ¹³⁹, M. Al-Turany ⁹⁷, D. Aleksandrov ¹³⁹, B. Alessandro ⁵⁵, H.M. Alfanda ⁶, R. Alfaro Molina ⁶⁶, B. Ali ¹⁵, Y. Ali¹³, A. Alici ²⁵, N. Alizadehvandchali ¹¹², A. Alkin ³², J. Alme ²⁰, G. Alocco ⁵¹, T. Alt ⁶³, I. Altsybeev ¹³⁹, M.N. Anaam ⁶, C. Andrei ⁴⁵, A. Andronic ¹³⁴, V. Anguelov ⁹⁴, F. Antinori ⁵³, P. Antonioli ⁵⁰, C. Anuj ¹⁵, N. Apadula ⁷³, L. Aphecetche ¹⁰², H. Appelshäuser ⁶³, S. Arcelli ²⁵, R. Arnaldi ⁵⁵, I.C. Arsene ¹⁹, M. Arslanok ¹³⁶, A. Augustinus ³², R. Averbeck ⁹⁷, S. Aziz ¹²⁷, M.D. Azmi ¹⁵, A. Badalà ⁵², Y.W. Baek ⁴⁰, X. Bai ⁹⁷, R. Bailhache ⁶³, Y. Bailung ⁴⁷, R. Bala ⁹⁰, A. Balbino ²⁹, A. Baldisseri ¹²⁶, B. Balis ², D. Banerjee ⁴, Z. Banoo ⁹⁰, R. Barbera ²⁶, L. Barioglio ⁹⁵, M. Barlou⁷⁷, G.G. Barnaföldi ¹³⁵, L.S. Barnby ⁸⁴, V. Barret ¹²³, L. Barreto ¹⁰⁸, C. Bartels ¹¹⁵, K. Barth ³², E. Bartsch ⁶³, F. Baruffaldi ²⁷, N. Bastid ¹²³, S. Basu ⁷⁴, G. Batigne ¹⁰², D. Battistini ⁹⁵, B. Batyunya ¹⁴⁰, D. Bauri⁴⁶, J.L. Bazo Alba ¹⁰⁰, I.G. Bearden ⁸², C. Beattie ¹³⁶, P. Becht ⁹⁷, D. Behera ⁴⁷, I. Belikov ¹²⁵, A.D.C. Bell Hechavarria ¹³⁴, F. Bellini ²⁵, R. Bellwied ¹¹², S. Belokurova ¹³⁹, V. Belyaev ¹³⁹, G. Bencedi ^{135,64}, S. Beole ²⁴, A. Bercuci ⁴⁵, Y. Berdnikov ¹³⁹, A. Berdnikova ⁹⁴, L. Bergmann ⁹⁴, M.G. Besoiu ⁶², L. Betev ³², P.P. Bhaduri ¹³¹, A. Bhasin ⁹⁰, I.R. Bhat⁹⁰, M.A. Bhat ⁴, B. Bhattacharjee ⁴¹, L. Bianchi ²⁴, N. Bianchi ⁴⁸, J. Bielčik ³⁵, J. Bielčíková ⁸⁵, J. Biernat ¹⁰⁵, A. Bilandzic ⁹⁵, G. Biro ¹³⁵, S. Biswas ⁴, J.T. Blair ¹⁰⁶, D. Blau ¹³⁹, M.B. Blidaru ⁹⁷, N. Bluhme³⁸, C. Blume ⁶³, G. Boca ^{21,54}, F. Bock ⁸⁶, T. Bodova ²⁰, A. Bogdanov¹³⁹, S. Boi ²², J. Bok ⁵⁷, L. Boldizsár ¹³⁵, A. Bolozdynya ¹³⁹, M. Bombara ³⁷, P.M. Bond ³², G. Bonomi ^{130,54}, H. Borel ¹²⁶, A. Borissov ¹³⁹, H. Bossi ¹³⁶, E. Botta ²⁴, L. Bratrud ⁶³, P. Braun-Munzinger ⁹⁷, M. Bregant ¹⁰⁸, M. Broz ³⁵, G.E. Bruno ^{96,31}, M.D. Buckland ¹¹⁵, D. Budnikov ¹³⁹, H. Buesching ⁶³, S. Bufalino ²⁹, O. Bugnon¹⁰², P. Buhler ¹⁰¹, Z. Buthelezi ^{67,119}, J.B. Butt¹³, A. Bylinkin ¹¹⁴, S.A. Bysiak¹⁰⁵, M. Cai ^{27,6}, H. Caines ¹³⁶, A. Caliva ⁹⁷, E. Calvo Villar ¹⁰⁰, J.M.M. Camacho ¹⁰⁷, P. Camerini ²³, F.D.M. Canedo ¹⁰⁸, M. Carabas ¹²², F. Carnesecchi ³², R. Caron ^{124,126}, J. Castillo Castellanos ¹²⁶, F. Catalano ²⁹, C. Ceballos Sanchez ¹⁴⁰, I. Chakaberia ⁷³, P. Chakraborty ⁴⁶, S. Chandra ¹³¹, S. Chapeland ³², M. Chartier ¹¹⁵, S. Chattopadhyay ¹³¹, S. Chattopadhyay ⁹⁸, T.G. Chavez ⁴⁴, T. Cheng ⁶, C. Cheshkov ¹²⁴, B. Cheynis ¹²⁴, V. Chibante Barroso ³², D.D. Chinellato ¹⁰⁹, E.S. Chizzali ^{11,95}, J. Cho ⁵⁷, S. Cho ⁵⁷, P. Chochula ³², P. Christakoglou ⁸³, C.H. Christensen ⁸², P. Christiansen ⁷⁴, T. Chujo ¹²¹, M. Ciacco ²⁹, C. Cicalo ⁵¹, L. Cifarelli ²⁵, F. Cindolo ⁵⁰, M.R. Ciupek⁹⁷, G. Clai^{III,50}, F. Colamaria ⁴⁹, J.S. Colburn⁹⁹, D. Colella ^{96,31}, A. Collu⁷³, M. Colocci ³², M. Concas ^{IV,55}, G. Conesa Balbastre ⁷², Z. Conesa del Valle ¹²⁷, G. Contin ²³, J.G. Contreras ³⁵, M.L. Coquet ¹²⁶, T.M. Cormier^{1,86}, P. Cortese ^{129,55}, M.R. Cosentino ¹¹⁰, F. Costa ³², S. Costanza ^{21,54}, P. Crochet ¹²³, R. Cruz-Torres ⁷³, E. Cuautle⁶⁴, P. Cui ⁶, L. Cunquero ⁸⁶, A. Dainese ⁵³, M.C. Danisch ⁹⁴, A. Danu ⁶², P. Das ⁷⁹, P. Das ⁴, S. Das ⁴, A.R. Dash ¹³⁴, S. Dash ⁴⁶, R.M.H. David⁴⁴, A. De Caro ²⁸, G. de Cataldo ⁴⁹, L. De Cilladi ²⁴, J. de Cuveland³⁸, A. De Falco ²², D. De Gruttola ²⁸, N. De Marco ⁵⁵, C. De Martin ²³, S. De Pasquale ²⁸, S. Deb ⁴⁷, H.F. Degenhardt¹⁰⁸, K.R. Deja ¹³², R. Del Grande ⁹⁵, L. Dello Stritto ²⁸, W. Deng ⁶, P. Dhankher ¹⁸, D. Di Bari ³¹, A. Di Mauro ³², R.A. Diaz ^{140,7}, T. Dietel ¹¹¹, Y. Ding ^{124,6}, R. Divià ³², D.U. Dixit ¹⁸, Ø. Djuvsland²⁰, U. Dmitrieva ¹³⁹, A. Dobrin ⁶², B. Dönigus ⁶³, A.K. Dubey ¹³¹, J.M. Dubinski ¹³², A. Dubla ⁹⁷, S. Dudi ⁸⁹, P. Dupieux ¹²³, M. Durkac¹⁰⁴, N. Dzalaiova¹², T.M. Eder ¹³⁴, R.J. Ehlers ⁸⁶, V.N. Eikeland²⁰, F. Eisenhut ⁶³, D. Elia ⁴⁹, B. Erasmus ¹⁰², F. Ercolessi ²⁵, F. Erhardt ⁸⁸, M.R. Ersdal²⁰, B. Espagnon ¹²⁷, G. Eulisse ³², D. Evans ⁹⁹, S. Evdokimov ¹³⁹, L. Fabbietti ⁹⁵, M. Faggin ²⁷, J. Faivre ⁷², F. Fan ⁶, W. Fan ⁷³, A. Fantoni ⁴⁸, M. Fasel ⁸⁶, P. Fedchio²⁹, A. Feliciello ⁵⁵, G. Feofilov ¹³⁹, A. Fernández Téllez ⁴⁴, M.B. Ferrer ³², A. Ferrero ¹²⁶, A. Ferretti ²⁴, V.J.G. Feuillard ⁹⁴, J. Figiel ¹⁰⁵, V. Filova ³⁵, D. Finogeev ¹³⁹, F.M. Fionda ⁵¹, G. Fiorenza⁹⁶, F. Flor ¹¹², A.N. Flores ¹⁰⁶, S. Foertsch ⁶⁷, I. Fokin ⁹⁴, S. Fokin ¹³⁹, E. Fragiaco ⁵⁶, E. Frajna ¹³⁵, U. Fuchs ³², N. Funicello ²⁸, C. Furget ⁷², A. Furs ¹³⁹, J.J. Gaardhøje ⁸², M. Gagliardi ²⁴, A.M. Gago ¹⁰⁰, A. Gal¹²⁵, C.D. Galvan ¹⁰⁷, P. Ganoti ⁷⁷, C. Garabatos ⁹⁷, J.R.A. Garcia ⁴⁴, E. Garcia-Solis ⁹, K. Garg ¹⁰², C. Gargiulo ³², A. Garibli⁸⁰, K. Garner¹³⁴, E.F. Gauger ¹⁰⁶, A. Gautam ¹¹⁴, M.B. Gay Ducati ⁶⁵, M. Germain ¹⁰², S.K. Ghosh⁴, M. Giacalone ²⁵, P. Gianotti ⁴⁸, P. Giubellino ^{97,55}, P. Giubilato ²⁷, A.M.C. Glaenger ¹²⁶, P. Glässel ⁹⁴, E. Glimos ¹¹⁸, D.J.Q. Goh⁷⁵, V. Gonzalez ¹³³, L.H. González-Trueba ⁶⁶, S. Gorbunov³⁸, M. Gorgon ², L. Görlich ¹⁰⁵, S. Gotovac³³, V. Grabski ⁶⁶, L.K. Graczykowski ¹³², E. Grecka ⁸⁵, L. Greiner ⁷³, A. Grelli ⁵⁸, C. Grigoras ³², V. Grigoriev ¹³⁹, S. Grigoryan ^{140,1}, F. Grosa ³², J.F. Grosse-Oetringhaus ³², R. Grosso ⁹⁷, D. Grund ³⁵, G.G. Guardiano ¹⁰⁹, R. Guernane ⁷², M. Guilbaud ¹⁰², K. Gulbrandsen ⁸², T. Gunji ¹²⁰, W. Guo ⁶,

A. Gupta ⁹⁰, R. Gupta ⁹⁰, S.P. Guzman ⁴⁴, L. Gyulai ¹³⁵, M.K. Habib⁹⁷, C. Hadjidakis ¹²⁷,
 H. Hamagaki ⁷⁵, M. Hamid⁶, Y. Han ¹³⁷, R. Hannigan ¹⁰⁶, M.R. Haque ¹³², A. Harlenderova⁹⁷,
 J.W. Harris ¹³⁶, A. Harton ⁹, J.A. Hasenbichler³², H. Hassan ⁸⁶, D. Hatzifotiadou ⁵⁰, P. Hauer ⁴²,
 L.B. Havener ¹³⁶, S.T. Heckel ⁹⁵, E. Hellbär ⁹⁷, H. Helstrup ³⁴, T. Herman ³⁵, G. Herrera Corral ⁸,
 F. Herrmann¹³⁴, K.F. Hetland ³⁴, B. Heybeck ⁶³, H. Hillemanns ³², C. Hills ¹¹⁵, B. Hippolyte ¹²⁵,
 B. Hofman ⁵⁸, B. Hohlweger ⁸³, J. Honermann ¹³⁴, G.H. Hong ¹³⁷, D. Horak ³⁵, A. Horzyk²,
 R. Hosokawa¹⁴, Y. Hou ⁶, P. Hristov ³², C. Hughes ¹¹⁸, P. Huhn⁶³, L.M. Huhta ¹¹³, C.V. Hulse ¹²⁷,
 T.J. Humanic ⁸⁷, H. Hushnud⁹⁸, A. Hutson ¹¹², D. Hutter ³⁸, J.P. Iddon ¹¹⁵, R. Ilkaev¹³⁹, H. Ilyas ¹³,
 M. Inaba ¹²¹, G.M. Innocenti ³², M. Ippolitov ¹³⁹, A. Isakov ⁸⁵, T. Isidori ¹¹⁴, M.S. Islam ⁹⁸,
 M. Ivanov ⁹⁷, V. Ivanov ¹³⁹, V. Izucheev¹³⁹, M. Jablonski ², B. Jacak ⁷³, N. Jacazio ³², P.M. Jacobs ⁷³,
 S. Jadlovská¹⁰⁴, J. Jadlovsky¹⁰⁴, L. Jaffe³⁸, C. Jahnke ¹⁰⁹, M.A. Janik ¹³², T. Janson⁶⁹, M. Jercic⁸⁸,
 O. Jevons⁹⁹, A.A.P. Jimenez ⁶⁴, F. Jonas ⁸⁶, P.G. Jones⁹⁹, J.M. Jowett ^{32,97}, J. Jung ⁶³, M. Jung ⁶³,
 A. Junique ³², A. Jusko ⁹⁹, M.J. Kabus ^{32,132}, J. Kaewjai¹⁰³, P. Kalinak ⁵⁹, A.S. Kalteyer ⁹⁷,
 A. Kalweit ³², V. Kaplin ¹³⁹, A. Karasu Uysal ⁷¹, D. Karatovic ⁸⁸, O. Karavichev ¹³⁹,
 T. Karavicheva ¹³⁹, P. Karczmarczyk ¹³², E. Karpechev ¹³⁹, V. Kashyap⁷⁹, A. Kazantsev¹³⁹,
 U. Keschull ⁶⁹, R. Keidel ¹³⁸, D.L.D. Keijdener⁵⁸, M. Keil ³², B. Ketzer ⁴², A.M. Khan ⁶, S. Khan ¹⁵,
 A. Khanzadeev ¹³⁹, Y. Kharlov ¹³⁹, A. Khatun ¹⁵, A. Khuntia ¹⁰⁵, B. Kileng ³⁴, B. Kim ¹⁶,
 C. Kim ¹⁶, D.J. Kim ¹¹³, E.J. Kim ⁶⁸, J. Kim ¹³⁷, J.S. Kim ⁴⁰, J. Kim ⁹⁴, J. Kim ⁶⁸, M. Kim ⁹⁴,
 S. Kim ¹⁷, T. Kim ¹³⁷, S. Kirsch ⁶³, I. Kisel ³⁸, S. Kiselev ¹³⁹, A. Kisiel ¹³², J.P. Kitowski ²,
 J.L. Klay ⁵, J. Klein ³², S. Klein ⁷³, C. Klein-Bösing ¹³⁴, M. Kleiner ⁶³, T. Klemenz ⁹⁵, A. Kluge ³²,
 A.G. Knospe ¹¹², C. Kobdaj ¹⁰³, T. Kollegger⁹⁷, A. Kondratyev ¹⁴⁰, N. Kondratyeva ¹³⁹,
 E. Kondratyuk ¹³⁹, J. Konig ⁶³, S.A. Konigstorfer ⁹⁵, P.J. Konopka ³², G. Kornakov ¹³²,
 S.D. Koryciak ², A. Kotliarov ⁸⁵, O. Kovalenko ⁷⁸, V. Kovalenko ¹³⁹, M. Kowalski ¹⁰⁵, I. Králík ⁵⁹,
 A. Kravčáková ³⁷, L. Kreis⁹⁷, M. Krivda ^{99,59}, F. Krizek ⁸⁵, K. Krizkova Gajdosova ³⁵, M. Kroesen ⁹⁴,
 M. Krüger ⁶³, D.M. Krupova ³⁵, E. Kryshen ¹³⁹, M. Krzewicki³⁸, V. Kučera ³², C. Kuhn ¹²⁵,
 P.G. Kuijjer ⁸³, T. Kumaoka¹²¹, D. Kumar¹³¹, L. Kumar ⁸⁹, N. Kumar⁸⁹, S. Kundu ³², P. Kurashvili ⁷⁸,
 A. Kurepin ¹³⁹, A.B. Kurepin ¹³⁹, S. Kuschpil ⁸⁵, J. Kvapil ⁹⁹, M.J. Kweon ⁵⁷, J.Y. Kwon ⁵⁷,
 Y. Kwon ¹³⁷, S.L. La Pointe ³⁸, P. La Rocca ²⁶, Y.S. Lai⁷³, A. Lakrathok¹⁰³, M. Lamanna ³²,
 R. Langoy ¹¹⁷, P. Larionov ⁴⁸, E. Laudi ³², L. Lautner ^{32,95}, R. Lavicka ¹⁰¹, T. Lazareva ¹³⁹,
 R. Lea ^{130,54}, G. Legras ¹³⁴, J. Lehrbach ³⁸, R.C. Lemmon ⁸⁴, I. León Monzón ¹⁰⁷, M.M. Lesch ⁹⁵,
 E.D. Lesser ¹⁸, M. Lettrich⁹⁵, P. Lévai ¹³⁵, X. Li¹⁰, X.L. Li⁶, J. Lien ¹¹⁷, R. Lietava ⁹⁹, B. Lim ¹⁶,
 S.H. Lim ¹⁶, V. Lindenstruth ³⁸, A. Lindner⁴⁵, C. Lippmann ⁹⁷, A. Liu ¹⁸, D.H. Liu ⁶, J. Liu ¹¹⁵,
 I.M. Lofnes ²⁰, V. Logunov¹³⁹, C. Loizides ⁸⁶, P. Loncar³³, J.A. Lopez ⁹⁴, X. Lopez ¹²³, E. López
 Torres ⁷, P. Lu ^{97,116}, J.R. Luhder ¹³⁴, M. Lunardon ²⁷, G. Luparello ⁵⁶, Y.G. Ma ³⁹, A. Maevskaya¹³⁹,
 M. Mager ³², T. Mahmoud⁴², A. Maire ¹²⁵, M. Malaev ¹³⁹, N.M. Malik ⁹⁰, Q.W. Malik¹⁹, S.K. Malik ⁹⁰,
 L. Malinina ^{VII,140}, D. Mal'Kevich ¹³⁹, D. Mallick ⁷⁹, N. Mallick ⁴⁷, G. Mandaglio ^{30,52}, V. Manko ¹³⁹,
 F. Manso ¹²³, V. Manzari ⁴⁹, Y. Mao ⁶, G.V. Margagliotti ²³, A. Margotti ⁵⁰, A. Marín ⁹⁷,
 C. Markert ¹⁰⁶, M. Marquard⁶³, N.A. Martin⁹⁴, P. Martinengo ³², J.L. Martinez¹¹², M.I. Martínez ⁴⁴,
 G. Martínez García ¹⁰², S. Masciocchi ⁹⁷, M. Masera ²⁴, A. Masoni ⁵¹, L. Massacrier ¹²⁷,
 A. Mastroserio ^{128,49}, A.M. Mathis ⁹⁵, O. Matonoha ⁷⁴, P.F.T. Matuoka¹⁰⁸, A. Matyja ¹⁰⁵, C. Mayer ¹⁰⁵,
 A.L. Mazuecos ³², F. Mazzaschi ²⁴, M. Mazzilli ³², J.E. Mdhuli ¹¹⁹, A.F. Mechler⁶³, Y. Melikyan ¹³⁹,
 A. Menchaca-Rocha ⁶⁶, E. Meninno ^{101,28}, A.S. Menon ¹¹², M. Meres ¹², S. Mhlanga^{111,67}, Y. Miake¹²¹,
 L. Micheletti ⁵⁵, L.C. Migliorin¹²⁴, D.L. Mihaylov ⁹⁵, K. Mikhaylov ^{140,139}, A.N. Mishra ¹³⁵,
 D. Miśkowiec ⁹⁷, A. Modak ⁴, A.P. Mohanty ⁵⁸, B. Mohanty⁷⁹, M. Mohisin Khan ^{V,15},
 M.A. Molander ⁴³, Z. Moravcova ⁸², C. Mordasini ⁹⁵, D.A. Moreira De Godoy ¹³⁴, I. Morozov ¹³⁹,
 A. Morsch ³², T. Mrnjavac ³², V. Muccifora ⁴⁸, E. Mudnic³³, S. Muhuri ¹³¹, J.D. Mulligan ⁷³,
 A. Mulliri²², M.G. Munhoz ¹⁰⁸, R.H. Munzer ⁶³, H. Murakami ¹²⁰, S. Murray ¹¹¹, L. Musa ³²,
 J. Musinsky ⁵⁹, J.W. Myrcha ¹³², B. Naik ¹¹⁹, R. Nair ⁷⁸, B.K. Nandi ⁴⁶, R. Nania ⁵⁰, E. Nappi ⁴⁹,
 A.F. Nassirpour ⁷⁴, A. Nath ⁹⁴, C. Nattrass ¹¹⁸, A. Neagu¹⁹, A. Negru¹²², L. Nellen ⁶⁴, S.V. Nesbo³⁴,
 G. Neskovic ³⁸, D. Nesterov ¹³⁹, B.S. Nielsen ⁸², E.G. Nielsen ⁸², S. Nikolaev ¹³⁹, S. Nikulin ¹³⁹,
 V. Nikulin ¹³⁹, F. Noferini ⁵⁰, S. Noh ¹¹, P. Nomokonov ¹⁴⁰, J. Norman ¹¹⁵, N. Novitzky ¹²¹,
 P. Nowakowski ¹³², A. Nyanin ¹³⁹, J. Nystrand ²⁰, M. Ogino ⁷⁵, A. Ohlson ⁷⁴, V.A. Okorokov ¹³⁹,
 J. Olińczak ¹³², A.C. Oliveira Da Silva ¹¹⁸, M.H. Oliver ¹³⁶, A. Onnerstad ¹¹³, C. Oppedisano ⁵⁵,
 A. Ortiz Velasquez ⁶⁴, A. Oskarsson⁷⁴, J. Otwinowski ¹⁰⁵, M. Oya⁹², K. Oyama ⁷⁵, Y. Pachmayer ⁹⁴,
 S. Padhan ⁴⁶, D. Pagano ^{130,54}, G. Paic ⁶⁴, A. Palasciano

L.G. Pereira ⁶⁵, H. Pereira Da Costa ¹²⁶, D. Peresunko ¹³⁹, G.M. Perez ⁷, S. Perrin ¹²⁶, Y. Pestov ¹³⁹, V. Petráček ³⁵, V. Petrov ¹³⁹, M. Petrovici ⁴⁵, R.P. Pezzi ^{102,65}, S. Piano ⁵⁶, M. Pikna ¹², P. Pillot ¹⁰², O. Pinazza ^{50,32}, L. Pinsky ¹¹², C. Pinto ^{95,26}, S. Pisano ⁴⁸, M. Płoskoń ⁷³, M. Planinic ⁸⁸, F. Pliquett ⁶³, M.G. Poghosyan ⁸⁶, S. Politano ²⁹, N. Poljak ⁸⁸, A. Pop ⁴⁵, S. Porteboeuf-Houssais ¹²³, J. Porter ⁷³, V. Pozdniakov ¹⁴⁰, S.K. Prasad ⁴, S. Prasad ⁴⁷, R. Preghenella ⁵⁰, F. Prino ⁵⁵, C.A. Pruneau ¹³³, I. Pshenichnov ¹³⁹, M. Puccio ³², Z. Pugelova ¹⁰⁴, S. Qiu ⁸³, L. Quaglia ²⁴, R.E. Quishpe ¹¹², S. Ragoni ⁹⁹, A. Rakotozafindrabe ¹²⁶, L. Ramello ^{129,55}, F. Rami ¹²⁵, S.A.R. Ramirez ⁴⁴, T.A. Rancien ⁷², R. Raniwala ⁹¹, S. Raniwala ⁹¹, S.S. Räsänen ⁴³, R. Rath ⁴⁷, I. Ravasenga ⁸³, K.F. Read ^{86,118}, A.R. Redelbach ³⁸, K. Redlich ^{VI,78}, A. Rehman ²⁰, P. Reichelt ⁶³, F. Reidt ³², H.A. Reme-Ness ³⁴, Z. Rescakova ³⁷, K. Reygers ⁹⁴, A. Riabov ¹³⁹, V. Riabov ¹³⁹, R. Ricci ²⁸, T. Richert ⁷⁴, M. Richter ¹⁹, W. Riegler ³², F. Riggi ²⁶, C. Ristea ⁶², M. Rodríguez Cahuantzi ⁴⁴, K. Røed ¹⁹, R. Rogalev ¹³⁹, E. Rogochaya ¹⁴⁰, T.S. Rogoschinski ⁶³, D. Rohr ³², D. Röhrich ²⁰, P.F. Rojas ⁴⁴, S. Rojas Torres ³⁵, P.S. Rokita ¹³², F. Ronchetti ⁴⁸, A. Rosano ^{30,52}, E.D. Rosas ⁶⁴, A. Rossi ⁵³, A. Roy ⁴⁷, P. Roy ⁹⁸, S. Roy ⁴⁶, N. Rubini ²⁵, D. Ruggiano ¹³², R. Rui ²³, B. Rumyantsev ¹⁴⁰, P.G. Russek ², R. Russo ⁸³, A. Rustamov ⁸⁰, E. Ryabinkin ¹³⁹, Y. Ryabov ¹³⁹, A. Rybicki ¹⁰⁵, H. Rytkonen ¹¹³, W. Rzesza ¹³², O.A.M. Saarimaki ⁴³, R. Sadek ¹⁰², S. Sadovsky ¹³⁹, J. Saetre ²⁰, K. Šafařík ³⁵, S.K. Saha ¹³¹, S. Saha ⁷⁹, B. Sahoo ⁴⁶, P. Sahoo ⁴⁶, R. Sahoo ⁴⁷, S. Sahoo ⁶⁰, D. Sahu ⁴⁷, P.K. Sahu ⁶⁰, J. Saini ¹³¹, K. Sajdakova ³⁷, S. Sakai ¹²¹, M.P. Salvan ⁹⁷, S. Sambyal ⁹⁰, T.B. Saramela ¹⁰⁸, D. Sarkar ¹³³, N. Sarkar ¹³¹, P. Sarma ⁴¹, V. Sarritzu ²², V.M. Sarti ⁹⁵, M.H.P. Sas ¹³⁶, J. Schambach ⁸⁶, H.S. Scheid ⁶³, C. Schiaua ⁴⁵, R. Schicker ⁹⁴, A. Schmah ⁹⁴, C. Schmidt ⁹⁷, H.R. Schmidt ⁹³, M.O. Schmidt ³², M. Schmidt ⁹³, N.V. Schmidt ^{86,63}, A.R. Schmier ¹¹⁸, R. Schotter ¹²⁵, J. Schukraft ³², K. Schwarz ⁹⁷, K. Schweda ⁹⁷, G. Scioli ²⁵, E. Scapparini ⁵⁵, J.E. Seger ¹⁴, Y. Sekiguchi ¹²⁰, D. Sekihata ¹²⁰, I. Selyuzhenkov ^{97,139}, S. Senyukov ¹²⁵, J.J. Seo ⁵⁷, D. Serebryakov ¹³⁹, L. Šerkšnytė ⁹⁵, A. Sevcenco ⁶², T.J. Shaba ⁶⁷, A. Shabanov ¹³⁹, A. Shabetai ¹⁰², R. Shahoyan ³², W. Shaikh ⁹⁸, A. Shangaraev ¹³⁹, A. Sharma ⁸⁹, D. Sharma ⁴⁶, H. Sharma ¹⁰⁵, M. Sharma ⁹⁰, N. Sharma ⁸⁹, S. Sharma ⁹⁰, U. Sharma ⁹⁰, A. Shatat ¹²⁷, O. Sheibani ¹¹², K. Shigaki ⁹², M. Shimomura ⁷⁶, S. Shirinkin ¹³⁹, Q. Shou ³⁹, Y. Sibiriak ¹³⁹, S. Siddhanta ⁵¹, T. Siemiarzuk ⁷⁸, T.F. Silva ¹⁰⁸, D. Silvermyr ⁷⁴, T. Simantathammakul ¹⁰³, R. Simeonov ³⁶, G. Simonetti ³², B. Singh ⁹⁰, B. Singh ⁹⁵, R. Singh ⁷⁹, R. Singh ⁹⁰, R. Singh ⁴⁷, V.K. Singh ¹³¹, V. Singhal ¹³¹, T. Sinha ⁹⁸, B. Sitar ¹², M. Sitta ^{129,55}, T.B. Skaali ¹⁹, G. Skorodumovs ⁹⁴, M. Slupecki ⁴³, N. Smirnov ¹³⁶, R.J.M. Snellings ⁵⁸, E.H. Solheim ¹⁹, C. Soncco ¹⁰⁰, J. Song ¹¹², A. Songmoolnak ¹⁰³, F. Soramel ²⁷, S.P. Sorensen ¹¹⁸, R. Soto Camacho ⁴⁴, R. Spijkers ⁸³, I. Sputowska ¹⁰⁵, J. Staa ⁷⁴, J. Stachel ⁹⁴, I. Stan ⁶², P.J. Steffanic ¹¹⁸, S.F. Stiefelmaier ⁹⁴, D. Stocco ¹⁰², I. Storehaug ¹⁹, M.M. Stortvedt ³⁴, P. Stratmann ¹³⁴, S. Strazzi ²⁵, C.P. Stylianidis ⁸³, A.A.P. Suaide ¹⁰⁸, C. Suire ¹²⁷, M. Sukhanov ¹³⁹, M. Suljic ³², V. Sumberia ⁹⁰, S. Sumowidagdo ⁸¹, S. Swain ⁶⁰, A. Szabo ¹², I. Szarka ¹², U. Tabassam ¹³, S.F. Taghavi ⁹⁵, G. Tallepied ^{97,123}, J. Takahashi ¹⁰⁹, G.J. Tambave ²⁰, S. Tang ^{123,6}, Z. Tang ¹¹⁶, J.D. Tapia Takaki ¹¹⁴, N. Tapus ¹²², L.A. Tarasovicova ¹³⁴, M.G. Tarzila ⁴⁵, G.F. Tassielli ³¹, A. Tauro ³², A. Telesca ³², L. Terlizzi ²⁴, C. Terrevoli ¹¹², G. Tersimonov ³, S. Thakur ¹³¹, D. Thomas ¹⁰⁶, R. Tieulent ¹²⁴, A. Tikhonov ¹³⁹, A.R. Timmins ¹¹², M. Tkacik ¹⁰⁴, T. Tkacik ¹⁰⁴, A. Toia ⁶³, N. Topilskaya ¹³⁹, M. Toppi ⁴⁸, F. Torales-Acosta ¹⁸, T. Tork ¹²⁷, A.G. Torres Ramos ³¹, A. Trifiró ^{30,52}, A.S. Triolo ^{30,52}, S. Tripathy ⁵⁰, T. Tripathy ⁴⁶, S. Trogolo ³², V. Trubnikov ³, W.H. Trzaska ¹¹³, T.P. Trzcinski ¹³², R. Turrisi ⁵³, T.S. Tveter ¹⁹, K. Ullaland ²⁰, B. Ulukutlu ⁹⁵, A. Uras ¹²⁴, M. Urioni ^{54,130}, G.L. Usai ²², M. Vala ³⁷, N. Valle ²¹, S. Vallero ⁵⁵, L.V.R. van Doremalen ⁵⁸, M. van Leeuwen ⁸³, C.A. van Veen ⁹⁴, R.J.G. van Weelden ⁸³, P. Vande Vyvre ³², D. Varga ¹³⁵, Z. Varga ¹³⁵, M. Varga-Kofarago ¹³⁵, M. Vasileiou ⁷⁷, A. Vasiliev ¹³⁹, O. Vázquez Doce ⁹⁵, O. Vazquez Rueda ⁷⁴, V. Vechernin ¹³⁹, E. Vercellin ²⁴, S. Vergara Limón ⁴⁴, L. Vermunt ⁵⁸, R. Vértesi ¹³⁵, M. Verweij ⁵⁸, L. Vickovic ³³, Z. Vilakazi ¹¹⁹, O. Villalobos Baillie ⁹⁹, G. Vino ⁴⁹, A. Vinogradov ¹³⁹, T. Virgili ²⁸, V. Vislavicius ⁸², A. Vodopyanov ¹⁴⁰, B. Volkel ³², M.A. Völkl ⁹⁴, K. Voloshin ¹³⁹, S.A. Voloshin ¹³³, G. Volpe ³¹, B. von Haller ³², I. Vorobyev ⁹⁵, N. Vozniuk ¹³⁹, J. Vrláková ³⁷, B. Wagner ²⁰, C. Wang ³⁹, D. Wang ³⁹, M. Weber ¹⁰¹, A. Wegrzynek ³², F.T. Weiglhofer ³⁸, S.C. Wenzel ³², J.P. Wessels ¹³⁴, S.L. Weyhiller ¹³⁶, J. Wiechula ⁶³, J. Wikne ¹⁹, G. Wilk ⁷⁸, J. Wilkinson ⁹⁷, G.A. Willems ¹³⁴, B. Windelband ⁹⁴, M. Winn ¹²⁶, J.R. Wright ¹⁰⁶, W. Wu ³⁹, Y. Wu ¹¹⁶, R. Xu ⁶, A.K. Yadav ¹³¹, S. Yalcin ⁷¹, Y. Yamaguchi ⁹², K. Yamakawa ⁹², S. Yang ²⁰, S. Yano ⁹², Z. Yin ⁶, I.-K. Yoo ¹⁶, J.H. Yoon ⁵⁷, S. Yuan ²⁰, A. Yuncu ⁹⁴, V. Zaccolo ²³, C. Zampolli ³², H.J.C. Zanoli ⁵⁸, F. Zanone ⁹⁴, N. Zardoshti ^{32,99}, A. Zarochentsev ¹³⁹, P. Závada ⁶¹, N. Zaviyalov ¹³⁹, M. Zhalov ¹³⁹, B. Zhang ⁶, S. Zhang ³⁹, X. Zhang ⁶, Y. Zhang ¹¹⁶, M. Zhao ¹⁰, V. Zherebchevskii ¹³⁹, Y. Zhi ¹⁰, N. Zhigareva ¹³⁹,

D. Zhou ⁶, Y. Zhou ⁸², J. Zhu ^{97,6}, Y. Zhu⁶, G. Zinovjev^{1,3}, N. Zurlo ^{130,54}

Affiliation Notes

^I Deceased

^{II} Also at: Max-Planck-Institut für Physik, Munich, Germany

^{III} Also at: Italian National Agency for New Technologies, Energy and Sustainable Economic Development (ENEA), Bologna, Italy

^{IV} Also at: Dipartimento DET del Politecnico di Torino, Turin, Italy

^V Also at: Department of Applied Physics, Aligarh Muslim University, Aligarh, India

^{VI} Also at: Institute of Theoretical Physics, University of Wrocław, Poland

^{VII} Also at: An institution covered by a cooperation agreement with CERN

Collaboration Institutes

¹ A.I. Alikhanyan National Science Laboratory (Yerevan Physics Institute) Foundation, Yerevan, Armenia

² AGH University of Krakow, Cracow, Poland

³ Bogolyubov Institute for Theoretical Physics, National Academy of Sciences of Ukraine, Kiev, Ukraine

⁴ Bose Institute, Department of Physics and Centre for Astroparticle Physics and Space Science (CAPSS), Kolkata, India

⁵ California Polytechnic State University, San Luis Obispo, California, United States

⁶ Central China Normal University, Wuhan, China

⁷ Centro de Aplicaciones Tecnológicas y Desarrollo Nuclear (CEADEN), Havana, Cuba

⁸ Centro de Investigación y de Estudios Avanzados (CINVESTAV), Mexico City and Mérida, Mexico

⁹ Chicago State University, Chicago, Illinois, United States

¹⁰ China Institute of Atomic Energy, Beijing, China

¹¹ Chungbuk National University, Cheongju, Republic of Korea

¹² Comenius University Bratislava, Faculty of Mathematics, Physics and Informatics, Bratislava, Slovak Republic

¹³ COMSATS University Islamabad, Islamabad, Pakistan

¹⁴ Creighton University, Omaha, Nebraska, United States

¹⁵ Department of Physics, Aligarh Muslim University, Aligarh, India

¹⁶ Department of Physics, Pusan National University, Pusan, Republic of Korea

¹⁷ Department of Physics, Sejong University, Seoul, Republic of Korea

¹⁸ Department of Physics, University of California, Berkeley, California, United States

¹⁹ Department of Physics, University of Oslo, Oslo, Norway

²⁰ Department of Physics and Technology, University of Bergen, Bergen, Norway

²¹ Dipartimento di Fisica, Università di Pavia, Pavia, Italy

²² Dipartimento di Fisica dell'Università and Sezione INFN, Cagliari, Italy

²³ Dipartimento di Fisica dell'Università and Sezione INFN, Trieste, Italy

²⁴ Dipartimento di Fisica dell'Università and Sezione INFN, Turin, Italy

²⁵ Dipartimento di Fisica e Astronomia dell'Università and Sezione INFN, Bologna, Italy

²⁶ Dipartimento di Fisica e Astronomia dell'Università and Sezione INFN, Catania, Italy

²⁷ Dipartimento di Fisica e Astronomia dell'Università and Sezione INFN, Padova, Italy

²⁸ Dipartimento di Fisica 'E.R. Caianiello' dell'Università and Gruppo Collegato INFN, Salerno, Italy

²⁹ Dipartimento DISAT del Politecnico and Sezione INFN, Turin, Italy

³⁰ Dipartimento di Scienze MIFT, Università di Messina, Messina, Italy

³¹ Dipartimento Interateneo di Fisica 'M. Merlin' and Sezione INFN, Bari, Italy

³² European Organization for Nuclear Research (CERN), Geneva, Switzerland

³³ Faculty of Electrical Engineering, Mechanical Engineering and Naval Architecture, University of Split, Split, Croatia

³⁴ Faculty of Engineering and Science, Western Norway University of Applied Sciences, Bergen, Norway

³⁵ Faculty of Nuclear Sciences and Physical Engineering, Czech Technical University in Prague, Prague, Czech Republic

³⁶ Faculty of Physics, Sofia University, Sofia, Bulgaria

³⁷ Faculty of Science, P.J. Šafárik University, Košice, Slovak Republic

³⁸ Frankfurt Institute for Advanced Studies, Johann Wolfgang Goethe-Universität Frankfurt, Frankfurt, Germany

- ³⁹ Fudan University, Shanghai, China
⁴⁰ Gangneung-Wonju National University, Gangneung, Republic of Korea
⁴¹ Gauhati University, Department of Physics, Guwahati, India
⁴² Helmholtz-Institut für Strahlen- und Kernphysik, Rheinische Friedrich-Wilhelms-Universität Bonn, Bonn, Germany
⁴³ Helsinki Institute of Physics (HIP), Helsinki, Finland
⁴⁴ High Energy Physics Group, Universidad Autónoma de Puebla, Puebla, Mexico
⁴⁵ Horia Hulubei National Institute of Physics and Nuclear Engineering, Bucharest, Romania
⁴⁶ Indian Institute of Technology Bombay (IIT), Mumbai, India
⁴⁷ Indian Institute of Technology Indore, Indore, India
⁴⁸ INFN, Laboratori Nazionali di Frascati, Frascati, Italy
⁴⁹ INFN, Sezione di Bari, Bari, Italy
⁵⁰ INFN, Sezione di Bologna, Bologna, Italy
⁵¹ INFN, Sezione di Cagliari, Cagliari, Italy
⁵² INFN, Sezione di Catania, Catania, Italy
⁵³ INFN, Sezione di Padova, Padova, Italy
⁵⁴ INFN, Sezione di Pavia, Pavia, Italy
⁵⁵ INFN, Sezione di Torino, Turin, Italy
⁵⁶ INFN, Sezione di Trieste, Trieste, Italy
⁵⁷ Inha University, Incheon, Republic of Korea
⁵⁸ Institute for Gravitational and Subatomic Physics (GRASP), Utrecht University/Nikhef, Utrecht, Netherlands
⁵⁹ Institute of Experimental Physics, Slovak Academy of Sciences, Košice, Slovak Republic
⁶⁰ Institute of Physics, Homi Bhabha National Institute, Bhubaneswar, India
⁶¹ Institute of Physics of the Czech Academy of Sciences, Prague, Czech Republic
⁶² Institute of Space Science (ISS), Bucharest, Romania
⁶³ Institut für Kernphysik, Johann Wolfgang Goethe-Universität Frankfurt, Frankfurt, Germany
⁶⁴ Instituto de Ciencias Nucleares, Universidad Nacional Autónoma de México, Mexico City, Mexico
⁶⁵ Instituto de Física, Universidade Federal do Rio Grande do Sul (UFRGS), Porto Alegre, Brazil
⁶⁶ Instituto de Física, Universidad Nacional Autónoma de México, Mexico City, Mexico
⁶⁷ iThemba LABS, National Research Foundation, Somerset West, South Africa
⁶⁸ Jeonbuk National University, Jeonju, Republic of Korea
⁶⁹ Johann-Wolfgang-Goethe Universität Frankfurt Institut für Informatik, Fachbereich Informatik und Mathematik, Frankfurt, Germany
⁷⁰ Korea Institute of Science and Technology Information, Daejeon, Republic of Korea
⁷¹ KTO Karatay University, Konya, Turkey
⁷² Laboratoire de Physique Subatomique et de Cosmologie, Université Grenoble-Alpes, CNRS-IN2P3, Grenoble, France
⁷³ Lawrence Berkeley National Laboratory, Berkeley, California, United States
⁷⁴ Lund University Department of Physics, Division of Particle Physics, Lund, Sweden
⁷⁵ Nagasaki Institute of Applied Science, Nagasaki, Japan
⁷⁶ Nara Women's University (NWU), Nara, Japan
⁷⁷ National and Kapodistrian University of Athens, School of Science, Department of Physics, Athens, Greece
⁷⁸ National Centre for Nuclear Research, Warsaw, Poland
⁷⁹ National Institute of Science Education and Research, Homi Bhabha National Institute, Jatni, India
⁸⁰ National Nuclear Research Center, Baku, Azerbaijan
⁸¹ National Research and Innovation Agency - BRIN, Jakarta, Indonesia
⁸² Niels Bohr Institute, University of Copenhagen, Copenhagen, Denmark
⁸³ Nikhef, National institute for subatomic physics, Amsterdam, Netherlands
⁸⁴ Nuclear Physics Group, STFC Daresbury Laboratory, Daresbury, United Kingdom
⁸⁵ Nuclear Physics Institute of the Czech Academy of Sciences, Husinec-Řež, Czech Republic
⁸⁶ Oak Ridge National Laboratory, Oak Ridge, Tennessee, United States
⁸⁷ Ohio State University, Columbus, Ohio, United States
⁸⁸ Physics department, Faculty of science, University of Zagreb, Zagreb, Croatia
⁸⁹ Physics Department, Panjab University, Chandigarh, India
⁹⁰ Physics Department, University of Jammu, Jammu, India
⁹¹ Physics Department, University of Rajasthan, Jaipur, India

- ⁹² Physics Program and International Institute for Sustainability with Knotted Chiral Meta Matter (SKCM2), Hiroshima University, Hiroshima, Japan
- ⁹³ Physikalisches Institut, Eberhard-Karls-Universität Tübingen, Tübingen, Germany
- ⁹⁴ Physikalisches Institut, Ruprecht-Karls-Universität Heidelberg, Heidelberg, Germany
- ⁹⁵ Physik Department, Technische Universität München, Munich, Germany
- ⁹⁶ Politecnico di Bari and Sezione INFN, Bari, Italy
- ⁹⁷ Research Division and ExtreMe Matter Institute EMMI, GSI Helmholtzzentrum für Schwerionenforschung GmbH, Darmstadt, Germany
- ⁹⁸ Saha Institute of Nuclear Physics, Homi Bhabha National Institute, Kolkata, India
- ⁹⁹ School of Physics and Astronomy, University of Birmingham, Birmingham, United Kingdom
- ¹⁰⁰ Sección Física, Departamento de Ciencias, Pontificia Universidad Católica del Perú, Lima, Peru
- ¹⁰¹ Stefan Meyer Institut für Subatomare Physik (SMI), Vienna, Austria
- ¹⁰² SUBATECH, IMT Atlantique, Nantes Université, CNRS-IN2P3, Nantes, France
- ¹⁰³ Suranaree University of Technology, Nakhon Ratchasima, Thailand
- ¹⁰⁴ Technical University of Košice, Košice, Slovak Republic
- ¹⁰⁵ The Henryk Niewodniczanski Institute of Nuclear Physics, Polish Academy of Sciences, Cracow, Poland
- ¹⁰⁶ The University of Texas at Austin, Austin, Texas, United States
- ¹⁰⁷ Universidad Autónoma de Sinaloa, Culiacán, Mexico
- ¹⁰⁸ Universidade de São Paulo (USP), São Paulo, Brazil
- ¹⁰⁹ Universidade Estadual de Campinas (UNICAMP), Campinas, Brazil
- ¹¹⁰ Universidade Federal do ABC, Santo Andre, Brazil
- ¹¹¹ University of Cape Town, Cape Town, South Africa
- ¹¹² University of Houston, Houston, Texas, United States
- ¹¹³ University of Jyväskylä, Jyväskylä, Finland
- ¹¹⁴ University of Kansas, Lawrence, Kansas, United States
- ¹¹⁵ University of Liverpool, Liverpool, United Kingdom
- ¹¹⁶ University of Science and Technology of China, Hefei, China
- ¹¹⁷ University of South-Eastern Norway, Kongsberg, Norway
- ¹¹⁸ University of Tennessee, Knoxville, Tennessee, United States
- ¹¹⁹ University of the Witwatersrand, Johannesburg, South Africa
- ¹²⁰ University of Tokyo, Tokyo, Japan
- ¹²¹ University of Tsukuba, Tsukuba, Japan
- ¹²² University Politehnica of Bucharest, Bucharest, Romania
- ¹²³ Université Clermont Auvergne, CNRS/IN2P3, LPC, Clermont-Ferrand, France
- ¹²⁴ Université de Lyon, CNRS/IN2P3, Institut de Physique des 2 Infinis de Lyon, Lyon, France
- ¹²⁵ Université de Strasbourg, CNRS, IPHC UMR 7178, F-67000 Strasbourg, France, Strasbourg, France
- ¹²⁶ Université Paris-Saclay, Centre d'Etudes de Saclay (CEA), IRFU, Département de Physique Nucléaire (DPhN), Saclay, France
- ¹²⁷ Université Paris-Saclay, CNRS/IN2P3, IJCLab, Orsay, France
- ¹²⁸ Università degli Studi di Foggia, Foggia, Italy
- ¹²⁹ Università del Piemonte Orientale, Vercelli, Italy
- ¹³⁰ Università di Brescia, Brescia, Italy
- ¹³¹ Variable Energy Cyclotron Centre, Homi Bhabha National Institute, Kolkata, India
- ¹³² Warsaw University of Technology, Warsaw, Poland
- ¹³³ Wayne State University, Detroit, Michigan, United States
- ¹³⁴ Westfälische Wilhelms-Universität Münster, Institut für Kernphysik, Münster, Germany
- ¹³⁵ Wigner Research Centre for Physics, Budapest, Hungary
- ¹³⁶ Yale University, New Haven, Connecticut, United States
- ¹³⁷ Yonsei University, Seoul, Republic of Korea
- ¹³⁸ Zentrum für Technologie und Transfer (ZTT), Worms, Germany
- ¹³⁹ Affiliated with an institute covered by a cooperation agreement with CERN
- ¹⁴⁰ Affiliated with an international laboratory covered by a cooperation agreement with CERN.